Front. Energy 2025, 19(4): 471–499
https://doi.org/10.1007/s11708-025-1010-8

REVIEW ARTICLE

Recent advances in high-entropy alloys for electrochemical hydrogen evolution, oxygen reduction, and CO_2 reduction reactions

Chao Zhang, Shengping You, Ang Du, Zewen Zhuang (✉), Wei Yan (✉), Jiujun Zhang (✉)

College of Materials Science and Engineering, Fujian Engineering Research Center of High Energy Batteries and New Energy Equipment & Systems, Fuzhou University, Fuzhou 350108, China

Abstract High entropy alloys (HEAs) have gained significant attention in electrocatalysis research due to their distinctive multi-element composition, intricate electronic structure, and superior properties. By harnessing multi-component synergy, precise electron regulation, and the high-entropy effect, HEA electrocatalysts exhibit remarkable catalytic activity, selectivity, and stability. These materials demonstrate outstanding catalytic performance in a variety of electrocatalytic small molecule reduction reactions, including oxygen reduction (ORR), hydrogen evolution (HER), and CO_2 reduction (CO_2RR), making them promising candidates for clean energy conversion and storage applications, including fuel cells, metal-air batteries, water electrolysis, and CO_2 conversion technologies. This review highlights recent advancements in HEA electrocatalyst research, focusing on their synthesis, characterization, and applications in electrocatalytic small molecule reduction reactions. It also explores the underlying mechanisms of the high-entropy effect, multi-component synergy, and structural design. Finally, it discusses key challenges that remain in the application of HEAs for electrocatalytic small molecule reduction and outlines potential directions for future development in this field.

Keywords high entropy alloys (HEAs), electrocatalysis, oxygen reduction reaction (ORR), CO_2 reduction reaction (CO_2RR), hydrogen evolution reaction (HER)

1 Introduction

The rapid advancement of science and technology has led to the extensive extraction and utilization of traditional fossil fuels to meet growing energy demands [1–4]. However, the consumption of these fossil fuels not only exacerbates the global energy shortage but also raises significant environmental and health concerns due to the substantial emissions of greenhouse gases and harmful pollutants [5,6]. Consequently, it is crucial to develop clean energy solutions and technologies that support sustainable development.

Green technologies have emerged as a promising strategy to address the dual challenges of energy shortages and environmental degradation caused by fossil fuel consumption. Among these, electrochemical energy conversion technologies have seen significant advancements, particularly in areas such as water electrolysis for hydrogen production, carbon dioxide reduction (CO_2RR), and the oxygen reduction reaction (ORR) [7–9]. Water electrolysis provides a clean and sustainable method for producing hydrogen, CO_2RR offers a pathway to convert greenhouse gases into valuable fuels, and ORR is widely applied in fuel cells and metal-air batteries, efficiently converting chemical energy into electrical energy. Collectively, these technologies play a crucial role in renewable energy utilization and storage. However, these small-molecule electrocatalytic reduction reactions require highly efficient and stable catalysts. The commonly used precious metal catalysts, such as Pt, Pd, and Ru, are limited by their high cost and scarcity, inhibiting their broad adoption [10–12]. Therefore, the development of

Received Jan. 16, 2025; accepted Mar. 30, 2025; online Jun. 10, 2025
Correspondences: Zewen Zhuang, zwzhuang@fzu.edu.cn;
Wei Yan, weiyan@fzu.edu.cn;
Jiujun Zhang, jiujun.zhang@fzu.edu.cn

cost-effective, high-performance electrocatalysts based on low-precious or non-precious metals has become a critical research priority [13–15].

High-entropy alloys (HEAs) represent a groundbreaking advancement in material science, redefining the traditional alloy design principles [16–18]. Unlike conventional alloys, which typically rely on one or two main elements, HEAs are composed of multiple principal elements. This unique composition results in high configurational entropy, complex lattice structures, and enhanced properties such as superior catalytic activity and chemical stability, making HEAs a pivotal innovation for advanced material applications [19–21]. In electrocatalysis, HEAs hold tremendous potential due to their diverse chemical compositions and abundant surface-active sites. Their multi-component nature not only enables precise control over reaction pathways but also enhances catalytic activity through tailored regulation of electronic structures [22,23]. Additionally, their unique lattice distortion effect and excellent corrosion resistance contribute to their remarkable stability in harsh electrochemical environments. These advantages open new possibilities for the development of highly efficient and durable electrocatalytic materials [16,24,25].

Over the past decades, substantial progress has been made in investigating HEAs for electrocatalysis applications. Through the precise design and combination of elements, scientists have developed a series of highly efficient HEA catalysts [26,27]. However, several challenges remain [28–30]. For instance, the synthesis methods for HEAs are complex and costly, making large-scale production difficult. Moreover, the intricate composition of HEAs means that the relationship between their structure and performance is not yet fully understood, creating a demand for further optimization and design [31–35]. Additionally, the long-term durability and degradation mechanisms of HEAs under practical electrochemical conditions require further exploration.

This review explores the progress and future prospects of HEAs in small-molecule electrocatalytic reduction reactions (Fig. 1). It begins by introducing the core principles of HEAs, emphasizing their structural advantages as electrocatalysts. Next, it reviews the synthesis methodologies and advanced characterization techniques utilized in HEA research. It then highlights their applications in key electrocatalytic reactions, including HER, ORR, and CO_2RR. Finally, it critically analyzes the current challenges in the field and propose future directions for the development of HEA-based catalysts. This work aims to inspire innovative strategies for designing efficient and durable HEAs-based electrocatalytic systems.

2 Structural advantages of HEA electrocatalysts

HEAs offer significant advantages as electrocatalysts. Compared to traditional low-entropy alloys, HEA catalysts have the following unique characteristics:

Multiple active sites: The complex surfaces of HEAs provide various active sites, making them adaptable to different reactants and conditions, which enhances catalytic efficiency and selectivity [23,40].

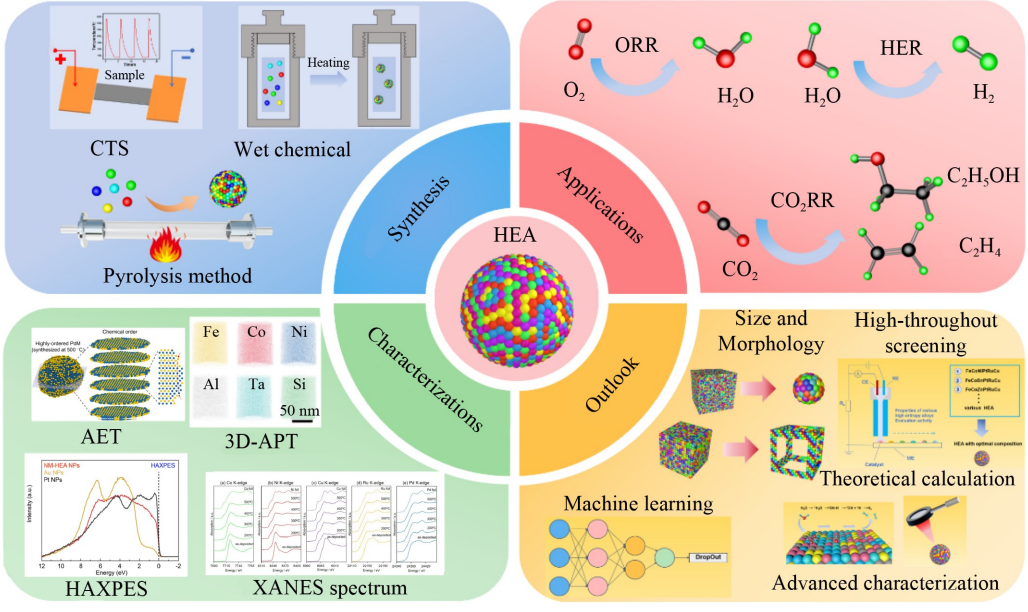

Fig. 1 Advances in HEA electrocatalysts.

(a) Synthesis methods; (b) characterization; (c) applications; (d) prospects (adapted with permission from Ref. [36–39], copyright 2024, Springer Nature, copyright 2021, Springer Nature, copyright 2024, ACS Publications).

Lattice distortion: Lattice distortion can alter the electronic structure of the active sites, further tunning the adsorption energy of the key reactant and intermediates, thereby enhancing the activity [22,41,42].

Tunable performance: Their multi-element composition allows for flexible material design and precise performance tuning.

Excellent stability: The high-entropy effect improves corrosion resistance and overall durability [43–46].

Multiple active sites: The multi-active sites of HEAs refer to the diverse active sites formed on the catalyst surface due to the incorporation of multiple elements into the alloy matrix [22,41]. These active sites are characterized by varying adsorption energies and reaction activities, which endow HEAs with the capability to accommodate a wide range of reactants and reaction conditions in catalytic processes. This structural and functional diversity greatly improves the catalytic efficiency of HEAs. Particularly in cascade reactions, the distinctive structural properties of HEAs facilitates the formation of desired intermediate products at each reaction step, thereby achieving improved selectivity and efficiency. Due to the dissociation of intermediates between consecutive reaction steps and their potential re-adsorption at different active sites, the multi-active sites of HEAs ensures that the number of functional sites corresponds to the number of steps in cascade reactions. This structural adaptability significantly enhances performance. For example, in the CO_2RR depicted in Fig. 2(a), varying adsorption energies of different active sites on HEAs favor the formation of CO intermediates while simultaneously suppressing the hydrogen evolution reaction. This selective inhibition ensures that the reaction proceeds in the desired path. In subsequent reaction steps, the three-dimensional structural design of the catalyst enables stable capture of the generated CO intermediates at other active sites, which further promotes the reduction of CO into multi-carbon products such as ethylene and ethanol. The synergistic effects between different sites not only optimizes each step of the reaction but also improves the selectivity and diversity of the products.

Lattice distortion: Lattice distortion enhances the adsorption properties in electrocatalytic reactions by altering the electronic environment and electron density of active sites [49,50]. In electrocatalytic processes, optimal adsorption strength is crucial for ensuring efficient catalysis. According to Sabatier's theory, excessively strong adsorption prevents effective desorption of the reactant, while too weak adsorption diminishes its activation capacity. The high-entropy effect induced by lattice distortion can significantly alter

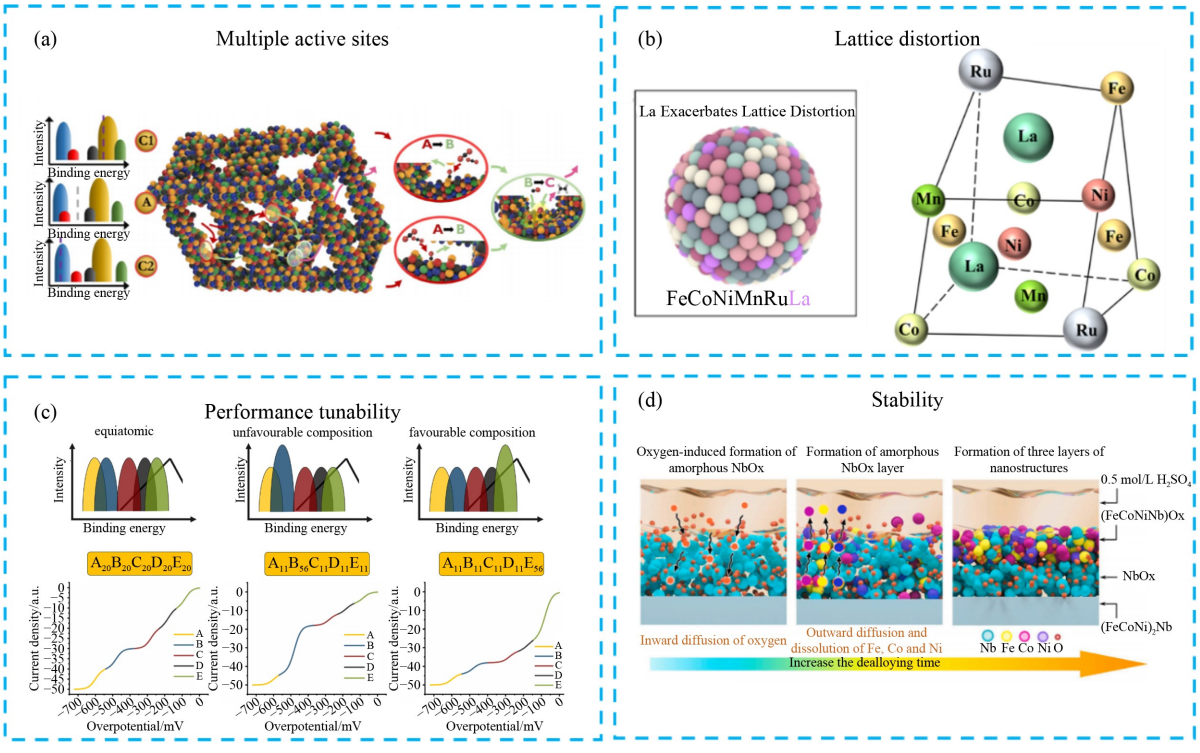

Fig. 2 Advantages of HEA.

(a) Multiple active sites trapping intermediates (adapted with permission from Löffler et al. [40], copyright 2021, Wiley); (b) lattice distortion changes catalytic reaction adsorption energy (adapted with permission from Wang et al. [47], copyright 2025, Elsevier); (c) performance tunability (adapted with permission from Löffler et al. [40], copyright 2021, Wiley); (d) high entropy effect inhibits active metal dissolution (adapted with permission from Li et al. [48], copyright 2024, Elsevier).

the electronic structure of the catalyst by influencing the electron overlap of the d orbitals. As shown in Fig. 2(b), Wang et al. [47] discovered that in the La-doped HEA FeCoNiMnRuLa, the introduction of La enhanced lattice distortion, which not only promoted d-d orbital electron transfer but also triggered a transition in the spin state of the d-orbital electrons from high spin to medium spin. The introduction of La in HEA catalysts adds to the overall lattice distortion effect, which optimizes the d-p orbital hybridization process, thereby significantly boosting OER activity.

Tunable performance: The tunability of HEAs origins from their diverse elemental composition and flexible structural design [51,52]. By adjusting the types, proportions, and structures of elements, the catalytic properties can be precisely optimized. In catalytic reactions, despite the broad adsorption energy distribution of adsorption energies on the HEA surface, the reaction process is primarily governed by strongly adsorptive active sites. The distribution of adsorption energies is significantly influenced by elemental electronic effects, interactions, and compositional adjustments. Optimizing the elemental composition regulates both the quantity and the nature of strong adsorption sites, enhancing catalytic activity and selectivity. For example, the catalytic performance is insignificant when five elements are distributed equally, in Fig. 2(c). Increasing the content of element B decreases activity, while increasing the content of element E significantly enhances activity. HEAs exhibit at least five binding peaks, whose intensity integrals are determined by the probability of binding atoms at the surface. As illustrated in the upper part of Fig. 2(c), increasing the molar ratio of a particular element correspondingly increases the number of sites within that binding peak. In the voltammogram (Fig. 2(c), bottom), the current is linearly proportional to the number of sites within the corresponding binding peak. Each color represents a different HEA composition, clearly demonstrating the electrocatalytic performance under various scenarios. Therefore, optimizing the molar ratios of co-binding elements at these sites increases the number of active sites [40].

Excellent stability: The alloy effect in HEAs significantly enhances the durability of catalysts [48,53,54]. As shown in Fig. 2(d), the presence of multiple elements in HEAs provides additional charge compensation centers, which alleviates strain on the active metal and reduces the potential for dissolution. This unique multi-element composition and highly mismatched lattice structure effectively enhance the durability and resistance to deactivation of the catalyst. The presence of multiple elements ensures additional charge compensation centers, which alleviates strain on the active metal and reduces the potential for dissolution. This stability is particularly important in highly corrosive environments, making HEAs ideal for harsh electrocatalytic applications [48].

In summary, the multi-component nature of HEAs facilitates the maximization of synergistic effects between multiple active sites, thereby refining the alloy's electronic configuration and lowering energy barriers associated with key reaction steps in the electrocatalysis process. These distinctive properties enable HEA catalysts to markedly enhance reaction performance, offering a robust material foundation for the development of efficient electrocatalysis technologies.

3 Synthetic method of HEA catalysts

Table 1 summarizes synthesis methods of HEA catalysts.

3.1 CTS

According to the thermodynamic formula, $\Delta G_{mix} = \Delta H_{mix} - T \times \Delta S_{mix}$, high-temperature condition facilitates the uniform distribution of different elements. However, slow cooling can lead to phase separation, resulting in the formation of multi-phase structures. To address this issue, high-temperature synthesis should be coupled with a rapid quenching process to ensure a balanced distribution of elements in a single-phase HEA catalyst.

The CTS method involves liquefying metal atoms through rapid high-temperature heating. During this process, the liquefied metal atoms undergo phenomena similar to "fission" and "fusion," resulting in the uniform mixing of various elements. Finally, rapid cooling enhances the kinetic regulation of the thermodynamic mixing process and supports the development of crystalline solid solution nanoparticles [58,59]. As illustrated in Fig. 3(a), Yao et al. [55] demonstrated this method by heating the precursor to 2000 K at a very rapid heating rate. The material was then cooled to room temperature at a cooling rate of 10^5 K/s, successfully synthesizing an eight-element HEA supported on a carbon matrix (Fig. 3(b)).

The CTS method is highly versatile, allowing the production of a variety of target materials by adjusting experimental parameters. For instance, Zeng et al. [56] synthesized a single-phase, homogeneous particle-size catalyst supported by commercial carbon black using a two-stage thermal shock procedure. In the first stage, rapid heating at ultra-high temperatures (1750 K, approximately 1 s) formed a non-noble metal HEAs core (NHEA). Subsequently, as shown in Fig. 3(c) and 3(d), a noble metal-modified HEA catalyst (NHEA@NHEA-Pd) was prepared by adding a precious metal salt (Pd) and subjecting the mixture to another round of rapid high-temperature heating (1118 K, approximately 0.3 s). The advantage of this catalyst is that there are more precious metal active sites exposed to the surface, while the internal HEA structure, composed of non-precious

Table 1 Summary of synthesis methods of HEA catalysts

Synthesis method	Description	Advantages	Disadvantages
CTS method	It rapidly heats the material by applying a high-intensity current over a short period, causing the material's own resistance to convert electrical energy into heat, enabling ultra-fast heating	The rapid heating and cooling process promotes fast alloying and prevents phase separation	The rapid heating and cooling process may lead to inconsistent diffusion rates, resulting in an uneven distribution of alloy composition
Wet-chemical method	The process denotes the reduction of metal precursors to alloys via solution-phase reactions	Solution environment is homogeneous, facilitating the uniform mixing of multiple metal elements	For certain metals that are difficult to dissolve or react, the wet-chemical method may not effectively achieve the desired alloying
Equilibrium pyrolysis method	By controlling temperature, time, atmosphere, and other conditions, the metal precursors undergo pyrolysis, leading to the formation of a homogeneous alloy with multiple metal elements in thermodynamic equilibrium	The temperature and reaction conditions are controllable; it is capable of forming structurally stable HEAs	The reaction time is relatively prolonged, making it difficult to achieve ultra-high temperature heating, and the process is characterized by high energy consumption
Non-equilibrium pyrolysis method	The process involves rapidly heating and controlling reaction conditions to allow the material to undergo pyrolysis in a non-equilibrium state	In the non-equilibrium state, uniform element distribution is achieved, minimizing phase separation, while alloying at elevated temperatures contributes to enhanced high-temperature stability	The reaction process is complex and difficult to control, with precise regulation the heating rate being challenging. Achieving ultra-high temperature pyrolysis conditions is a significant hurdle
Laser scanning ablation (LSA) method	By utilizing a high-energy laser beam to rapidly heat the target material, multiple metal elements can be swiftly mixed, leading to the formation of a HEA	The parameters such as laser energy, pulse frequency, and irradiation time can be precisely controlled, allowing for the adjustment of the alloy composition and microstructure	It is suitable for the preparation of small-scale samples, but it is challenging to meet the demands for large-scale, high-efficiency production due to high equipment requirements
Microwave heating method	The microwave heating method, through efficient electromagnetic heating, can promote the alloying reaction of HEAs in a short period	The microwave heating method enables uniform heating within a short time while providing precise control over particle size, composition, and structure, making it a promising technique for industrial applications	The material applicability is limited, particularly for materials with low dielectric constants, which may result in suboptimal heating efficiency
Sputtering deposition method	It involves ion bombardment of a solid target, causing atoms or molecules to detach and form a thin film on a substrate	The composition of the alloy films can be precisely controlled by adjusting the configuration of the sputtering sources, such as employing multi-target sputtering. Additionally, high-quality films with good uniformity can be fabricated on various substrates	The deposition rate of sputtering is generally lower compared to other methods, which may lead to reduced efficiency in large-scale production.
Freeze-thaw method	The freeze-thaw method for the preparation of HEAs involves dissolving metal salts, followed by freezing the solution to form a gel. The gel is then thawed and washed to remove impurities, and finally, freeze-dried to obtain an aerogel with high surface area	HEA aerogels prepared through the freeze-thaw method exhibit an excellent three-dimensional porous structure, which offers a high density of catalytic active sites	The freeze-thaw process necessitates precise control over temperature, time, and solution composition. Improper handling may result in instability in the quality of the aerogel, subsequently affecting its catalytic performance

metals, maintained high entropy and structure stability, greatly reducing the reliance on rare metals.

Yao et al. [57] further optimized the CTS method for high-flux preparation of HEAs (Fig. 3(e)). By loading different metal salts onto the heater, they enabled batch preparation of HEA. As shown in Fig. 3(f), transmission electron microscopy (TEM) images of the HEAs (PtPdRhRuIr) and (PtPdRhRuIrFeCo) clearly demonstrate the successful incorporation of the HEA and its uniform structure. This high-throughput approach offers an effective solution for the rapid preparation of multi-component HEAs.

Additionally, the CTS method enables precise control over the elemental composition of HEAs, offering a reliable means to investigate the impact of element ratios on catalyst performance. For instance, Xie et al. [58] developed a high-entropy ammonia decomposition catalyst using the CTS method. They successfully synthesized CoMoFeNiCu HEN at 2300 °C under thermal shock conditions by adjusting the Co and Mo content ratios. This approach allowed for precise control of the Co/Mo ratio, surpassing the mixability limits observed in conventional bimetallic Co–Mo catalysts. The CoMoFeNiCu HEA catalyst exhibited outstanding catalytic activity in ammonia decomposition, far surpassing the performance of rhodium-based catalyst.

3.2 Wet-chemistry methods

Wet-chemistry methods involve selecting the required soluble metal salts or oxides and preparing a solution based on the composition of the target material, ensuring that each element is present in its ionic or molecular form [60,61]. The metal ions are then uniformly precipitated or crystallized using techniques such as adding a precipitating agent, evaporation, sublimation, or hydrolysis, followed by processing the resulting material to yield the desired powder. However, for element

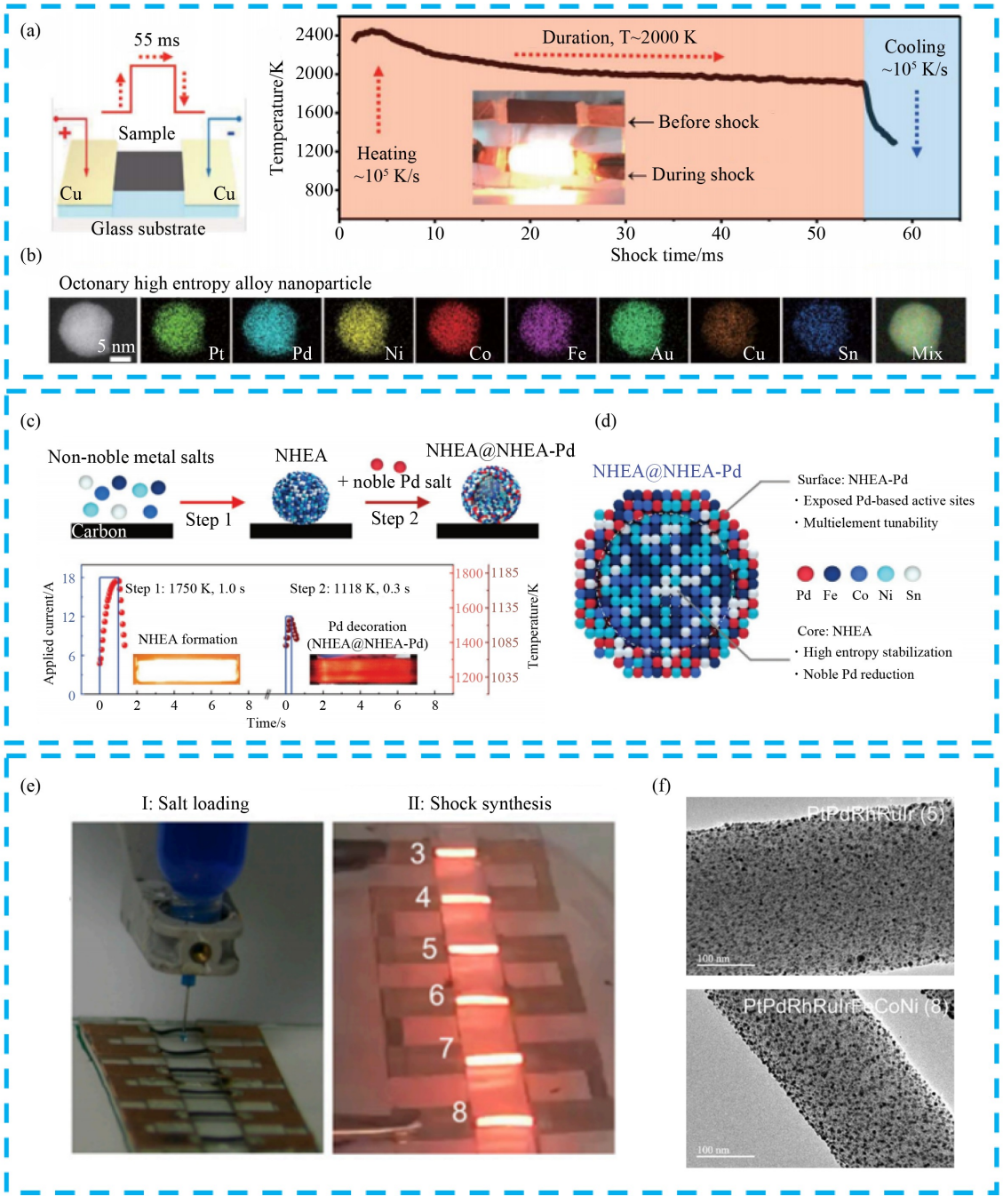

Fig. 3 Schematic diagram of the carbothermal shock (CTS) method.

(a) Synthesis process of CTS method and the temperature-time variation curve; (b) elemental mapping images of HEA nanoparticles composed of eight principal elements (adapted with permission from Yao et al. [55], copyright 2018, AAAS); (c) two-step carbothermal shock preparation process for HEAs; (d) structural diagram of a five-element HEA with a core-shell heterostructure (adapted with permission from Zeng et al. [56], copyright 2022, Wiley); (e) preparation process of multi-component HEAs: Step 1, liquid-phase composition design and deposition on a carbon carrier; Step 2, rapid thermal shock synthesis; (f) transmission electron microscopy (TEM) images of PtPdRhRuIr and PtPdRhRuIrFeCoNi HEAs (adapted with permission from Yao et al. [57], copyright 2020, National Academy of Sciences).

combinations that are slightly immiscible or require high uniformity, HEA nanoparticles synthesized using wet-chemical method present advantages including small particle size, accurate morphology, and uniform distribution, which are essential for achieving optimal catalytic performance.

In wet chemical synthesis, the solvent plays a pivotal role as the reaction medium, and its selection profoundly impacts the efficiency, quality, and performance of the final product. Oleylamine is widely used in wet chemical

synthesis due to its excellent thermal stability and ability to solubilize metal salts. For example, Luo et al. [62] employed five metallic carbonyl compounds ($M(CO)_x$, where M = Ir, Ru, Rh, Mo, W) as precursors (Fig. 4(a)). By utilizing oleylamine as the solvent and co-alloying the metals at 290 °C under an argon atmosphere, they successfully synthesized HEAs (IrRuRhMoW). The resulting catalyst exhibited outstanding electrocatalytic performance for HER in aqueous systems, demonstrating the effectiveness of this approach for fabricating high-performance materials. Similarly, He et al. [63] successfully synthesized FeCoNiPdWP HEAs using a mixed solvent of 1-octadecene and oleylamine, with metal acetylacetonates and carbonyl compounds as precursors, as illustrated in Fig. 4(b). In wet chemical preparation, the reduction and uniform deposition of metal ions can be enhanced by controlled heating, ultrasonic wave, the introduction of reducing agents and other auxiliary technologies, which significantly improve reaction efficiency, enable precise control over particle morphology, and mitigate component segregation. This method achieves the uniform distribution and precise synthesis of polymetallic HEA nanoparticles. Liu et al. [64] used an ultrasonic-assisted wet chemical method, creating acoustic cavitation to aid in the synthesis of five-element PtAuPdRhRu-NPs, four-element PtAuPdRh-NPs, and three-element PtAuPd-NPs, all supported on carbon support, under standard laboratory conditions, as shown in Fig. 4(c).

Nandan et al. [65] employed a one-pot method to synthesize PtPdRuMoNi mesoporous HEA nanospheres, as shown in Fig. 4(d). They first dissolved F-127 triblock copolymer in water, which formed a transparent solution containing micelles that acted as pore-forming agents.

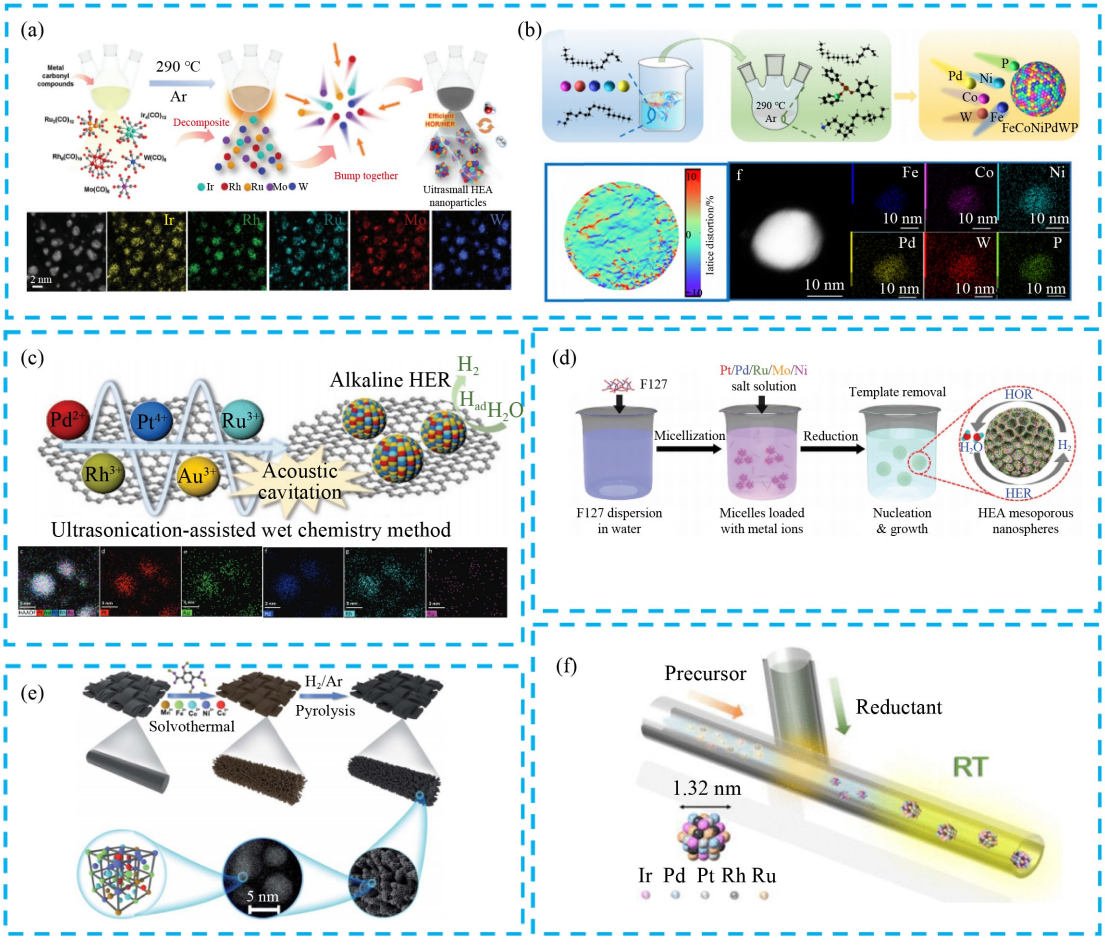

Fig. 4 Schematic diagrams of wet chemical methods.

(a) Oleylamine method for preparing IrRuRhMoW HEA (adapted with permission from Luo et al [62], copyright 2024, Wiley); (b) oleylamine method for preparing FeCoNiPdWP HEA (adapted with permission from He et al. [63], copyright 2024, RSC Publishing); (c) ultrasonic-assisted wet chemical method for preparing PdRhPtRuZu HEA (adapted with permission from Liu et al. [64], copyright 2019, Wiley); (d) mesoporous PtPdRuMoNi HEA prepared by wet chemical reduction with reducing agent (adapted with permission from Nandan et al. [65], copyright 2024, Wiley); (e) solvothermal method for preparing MnFeCoNiCu HEA (adapted with permission from Huang et al. [66], copyright 2020, RSC Publishing); (f) dchematic diagram of continuous flow method for preparing IrPdPtRhRu HEA (adapted with permission from Minamihara et al. [67], copyright 2022, ACS Publications).

The required metal salts were then added in the desired proportions, followed by the addition of ascorbic acid and hydrochloric acid to adjust the reduction potential of ascorbic acid and promote the nucleation process. After centrifugation, PtPdRuMoNi mesoporous HEA nanospheres were successfully obtained, exhibiting excellent activity for both the HER and hydrogen oxidation reaction in alkaline media. Huang et al. [66] used a solvothermal method to prepare MnFeCoNiCu HEA nanoparticles from a pentanuclear MOFs/CC precursor, as shown in Fig. 4(e). These nanoparticles, smaller than 5 nm, displayed a unique, interconnected structure due to the thin, highly conductive layers of graphitized carbon. Finally, Minamihara et al. [67] introduced a novel liquid-phase reduction method using lithium naphthalenide as a powerful reducing agent in a continuous-flow reactor, as depicted in Fig. 4(f). This approach successfully synthesized nano-scale IrPdPtRhRu HEA nanoparticles with sizes of 1.32 ± 0.41 nm. The continuous-flow reactor enables precise control over the reaction process, ensures stable reaction conditions, and guarantees high product selectivity and reproducibility. Additionally, by adjusting the strength of the reducing agent, the nanoparticle size can be effectively controlled, making this method one of the most efficient for producing uniformly sized, ultra-small HEA nanoparticles.

3.3 Pyrolysis

Pyrolysis is a thermal process in which organic or inorganic substances are subjected to high temperatures in an oxygen-deficient or low-oxygen environment, resulting in their chemical decomposition or transformation [68–70]. The typical temperature range for this method generally spans from 300 to 1000 °C. The synthesis of HEAs via pyrolysis generally involves two steps: the decomposition of metal precursors, and the subsequent reassembly of the resulting metals to form HEA nanoparticles [71]. By systematically regulating key parameters such as temperature, atmospheric composition, and reaction duration, it is possible to precisely control the particle size, morphology, and dispersion of the metallic components, thereby optimizing the catalyst's properties for specific applications.

Pyrolysis can be classified into two types based on the reaction conditions: equilibrium pyrolysis and non-equilibrium pyrolysis. In equilibrium pyrolysis, the reaction typically occurs under conditions that closely approach thermodynamic equilibrium. Specifically, factors like thermal conditions, pressure, and reaction duration are carefully regulated to ensure that the reaction achieves equilibrium. This balanced state represents the complete conversion of reactants into products under defined temperature and pressure conditions. In contrast, non-equilibrium pyrolysis occurs under conditions such as rapid heating or high temperatures maintained over short durations, where thermodynamic equilibrium is not achieved. This process typically takes place under dynamically fluctuating conditions. Non-equilibrium pyrolysis is characterized by elevated heating rates or high-temperature environments, where the distribution of reactants and products is primarily influenced by non-equilibrium factors, including reaction rates and temperature gradients.

3.3.1 Equilibrium pyrolysis

Kar et al. [72] proposed a strategy to convert two-phase core-shell metal nanoparticles into single-phase HEN through thermal annealing (Fig. 5(a)). Initially, intermetallic PdCu nanoparticles (i-PdCu, where i represents intermetallic compound, B2) were synthesized as seed particles. Upon heating, these seeds particles facilitated the co-reduction deposition of three metal shell layers (Pt, Ni, and M, where M represents Co, Fe, Ir, Rh, or Ru), resulting in the formation of HEA nanoparticles. This method reduces the amount of metal precursors required at each stage (seed synthesis and shell formation), thereby promoting the formation of monodisperse samples.

Similarly, Qiu et al. [73] proposed an optimal, universal pyrolysis-exchange-alloying method for preparing HEA nanoparticles (Fig. 5(b)). In this method, Co nanoparticles (NPs) are used as sacrificial templates. Metallic ions with higher oxidation potentials favor electron transfer from Co metal, leading to their deposition on the NP surface, which gives rise to the resulting CoRuPtIrRhPd HEA nanoparticles.

Zhang et al. [74] reported an anchoring-carbonization strategy that facilitates the creation of HEA nanocrystals (HENs) with sizes smaller than 3 nm, while simultaneously anchoring them onto ordered mesoporous carbon. During the preparation process, hydrophobic metal-organic compounds, the templating agent F127, and carbon precursors self-assemble into composite micelles through solvent evaporation, followed by curing at a low temperature. This is followed by calcination under a nitrogen atmosphere. As illustrated in Fig. 5 (c), when the temperature reaches the moderate range (below 400 °C), F127 evaporates, and the metal is reduced and anchored onto the partially carbonized framework. With the further increase in temperature, the framework undergoes additional carbonization, leading to the formation of planar contact between the HENs and the carbon, which strengthens their binding and prevents the dissolution, migration, or aggregation of the HENs at elevated temperatures. Using this method, HENs of different sizes, including 6, 7, 8, and 10 components (2.2, 2.6, 2.9, and 2.8 nm), were successfully synthesized. In electrocatalytic ORRs, the 6-component platinum-based HEA nanocrystals supported on porous carbon materials (PtNiFeCuCoZn Ns/PC) exhibited remarkable catalytic

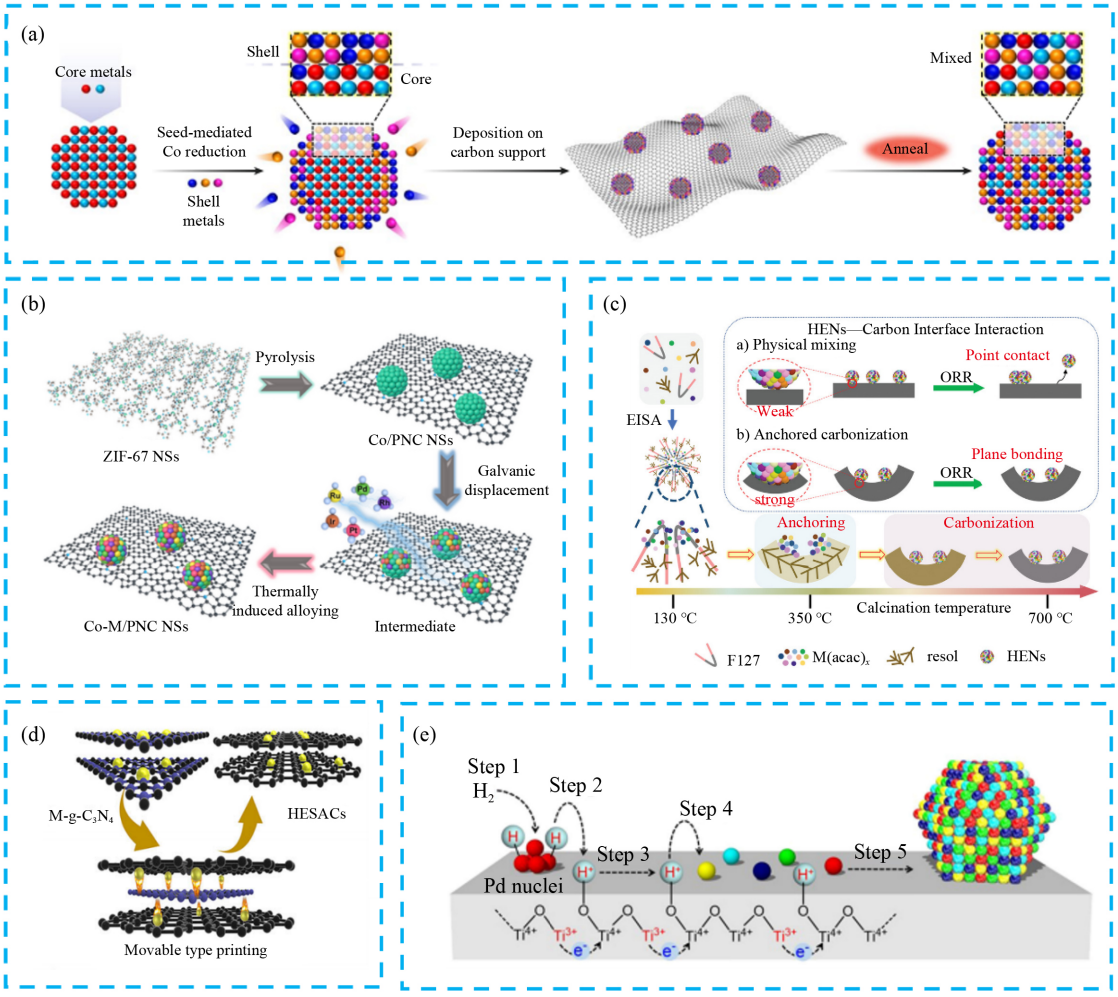

Fig. 5 Preparation of HEAs by equilibrium pyrolysis.

(a) HEA's formation with core-shell structures driven by high-temperature process (adapted with permission from Kar et al. [72], copyright 2023, Springer Nature); (b) preparation of the Co-M alloy/PNC NS (adapted with permission from Qiu et al. [73], copyright 2023, Wiley); (c) schematic diagram of the anchoring pyrolysis method for preparing HEA-carbon structures (adapted with permission from Zhang et al. [74], copyright 2022, Wiley); (d) schematic diagram of the movable printing method for preparing HESACs (adapted with permission from Rao et al. [75], copyright 2022, Springer Nature); (e) process flowchart of heat-driven hydrogen spillover for preparing HEA nanoparticles (adapted with permission from Mori et al. [76], copyright 2021, Springer Nature).

activity and durability.

As shown in Fig. 5(d), Rao et al. [75] developed a versatile and portable printing method. In this method, single metal atoms are transferred from a printing template onto a porous nitrogen-doped carbon support under thermal conditions, enabling the creation of HEN. By varying the printing molds and pyrolysis temperature, they successfully synthesized HEAs-supported atomic catalysts (HESACs) containing 5 to 11 metals. Notably, the five-metal HESAC catalyst (FeCoNiCuMn) demonstrated high efficiency in both the ORR and the zinc-air battery.

Hydrogen spillover refers to the process in which hydrogen molecules are adsorbed or dissociated on a catalyst's surface, converting into hydrogen atoms, which then migrate and diffuse to the catalyst support or neighboring materials. This phenomenon primarily occurs on metal catalyst surfaces, particularly those with a high hydrogen adsorption affinity for hydrogen adsorption, such as platinum, palladium, and nickel. It involves interactions between these metals and various supports, such as oxides or carbon materials. Mori et al. [76] employed a hydrogen spillover-driven synthesis strategy to develop a novel HEA nanoparticle catalyst. They demonstrated that titanium dioxide act as a potential medium for synthesizing non-equilibrium binary alloy nanoparticles, including RuNi and RhCu, which are naturally immiscible at equilibrium due to the positive formation enthalpy of solid-solution alloys (Fig. 5(e)). However, H_2 dissociates on the surface of Pd nuclei, forming reactive hydrogen atoms (H*) through the strong spillover effect of titanium dioxide, thereby enabling the

formation of highly specific binary alloy nanoparticles based on the combination of normally immiscible noble metals and alkali metals. The use of this oxide allows precious metals to generate hydrogen species with high reduction potential, which rapidly migrate and reduce alkali metals at low temperatures. Based on this characteristic, they successfully prepared CoNiCuRuPd HEA nanoparticles, which demonstrated high activity and excellent stability in CO_2RR.

3.3.2 Non-equilibrium pyrolysis

Compared to conventional pyrolysis methods, the fastmoving bed pyrolysis (FMBP) offers the advantages of rapid heating, enhanced gas–solid interaction, and excellent thermal transfer properties. These features make it highly suitable for producing high-performance catalysts, such as HEA nanoparticles and carbon-based catalysts. Gao et al. [77] utilized the FMBP method to successfully synthesize 2 nm-sized, ten-element MnCoNiCuRhPdSnIrPtAu HEA nanoparticles. As shown in Figs. 6(a) and 6(b), the process involved heating the furnace to 923 K under an inert argon atmosphere. A ceramic boat containing the precursor materials was then rapidly pushed toward the heating center at a velocity of 0.2 m/s, completing the pyrolysis process in just one second. The rapid, high-temperature procedure facilitated the concurrent heat-driven dissociation of the different metal precursors at a temperature exceeding the decomposition points of all individual components. The high supersaturation of monomers during this process promoted the formation of smaller nucleus aggregates, resulting in phase-separation-free HEA nanoparticles. They further illustrated the even distribution of elements within the synthesized nanoparticles. (Fig. 6(c)).

In a comparative experiment using the fixed bed pyrolysis (FBP) method, the precursors were heated slowly to 923 K, resulting in phase-separated alloys instead of HEAs. The FMBP method offers new perspectives for applying HEAs in catalytic fields, providing significant potential for applications in CO_2 conversion, hydrogenation reactions, and energy storage.

Wang et al. [78] reported a continuous "droplet-to-particle" method for synthesizing hollow HEA nanoparticles. By using a gas foaming agent combined with rapid high-temperature heating, hollow NiCoFeRuIr HEAs were successfully synthesized, uniformly incorporating up to eight different elements. The process and material formation are illustrated in Figs. 6(d) and 6(e).

In the method, aerosolized droplets containing metal precursors and a gas foaming agent are transported through a high-temperature zone using an inert carrier gas. As the droplets pass through this zone, the solvents and foaming agents rapidly evaporate and decompose, generating gas *in situ*, which causes the particles to expand into hollow structures. Subsequently, the metal precursors undergo thermal decomposition and alloying at elevated temperatures, resulting in uniform, single-phase HEA nanoparticles (Fig. 6(f)).

The process allows precise control over particle composition and structure, enabling customization of the HEA nanoparticles for specific applications.

3.4 Other synthesis methods

Wang et al. [79] proposed a simple and universal method,

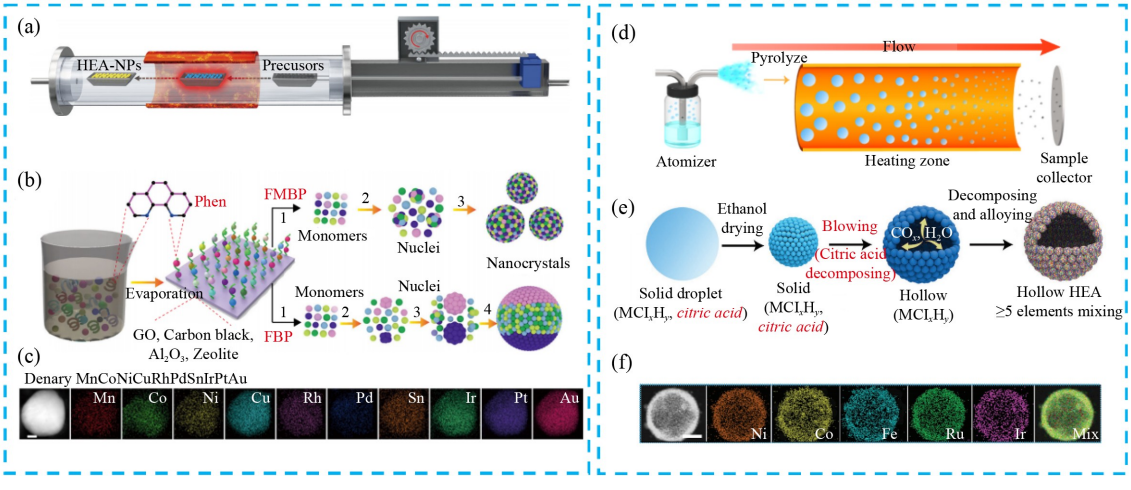

Fig. 6 Schematic diagrams of the non-equilibrium pyrolysis method for preparing HEA.

(a) Preparation of HEA-NPs by using the FMBP method; (b) differences in the preparation of HEAs using FMBP and FBP strategies; (c) element distribution map of the ten-element (MnCoNiCuRhPdSnIrPtAu) HEA-NPs (scale bar: 10 nm) (adapted with permission from Gao et al. [77], copyright 2020, Springer Nature); (d) schematic diagram of the process from droplet to particle; (e) schematic diagram of the droplet-to-particle evolution during the formation of hollow HEA particles; (f) STEM and EDS images of HEA RuIrFeCoNi nanoparticles (scale bar: 100 nm) (adapted with permission from Wang et al. [78], copyright 2020, Wiley).

laser synthesis and annealing (LSA) for synthesizing HEAs. This method offers the advantages of rapid and precise heating, ensuring the effective combination of different metal elements while enabling HEA nanoparticles to be loaded onto diverse substrates, including heat-sensitive materials, due to the laser pulse confining energy to the required micro-region. In this approach, they first loaded equimolar metal chlorides onto carbon nanotubes, then transferred the substrate to hexane and irradiated it with laser pulses at room temperature (Fig. 7(a)). By controlling the pulse power and width, they successfully prepared AuFeCoCuCr HEA nanoparticles on carbon nanotubes. They also employed different substrates such as graphene, copper foam, and glass and achieved uniformly distributed HEA nanoparticles on the surfaces of these substrates,

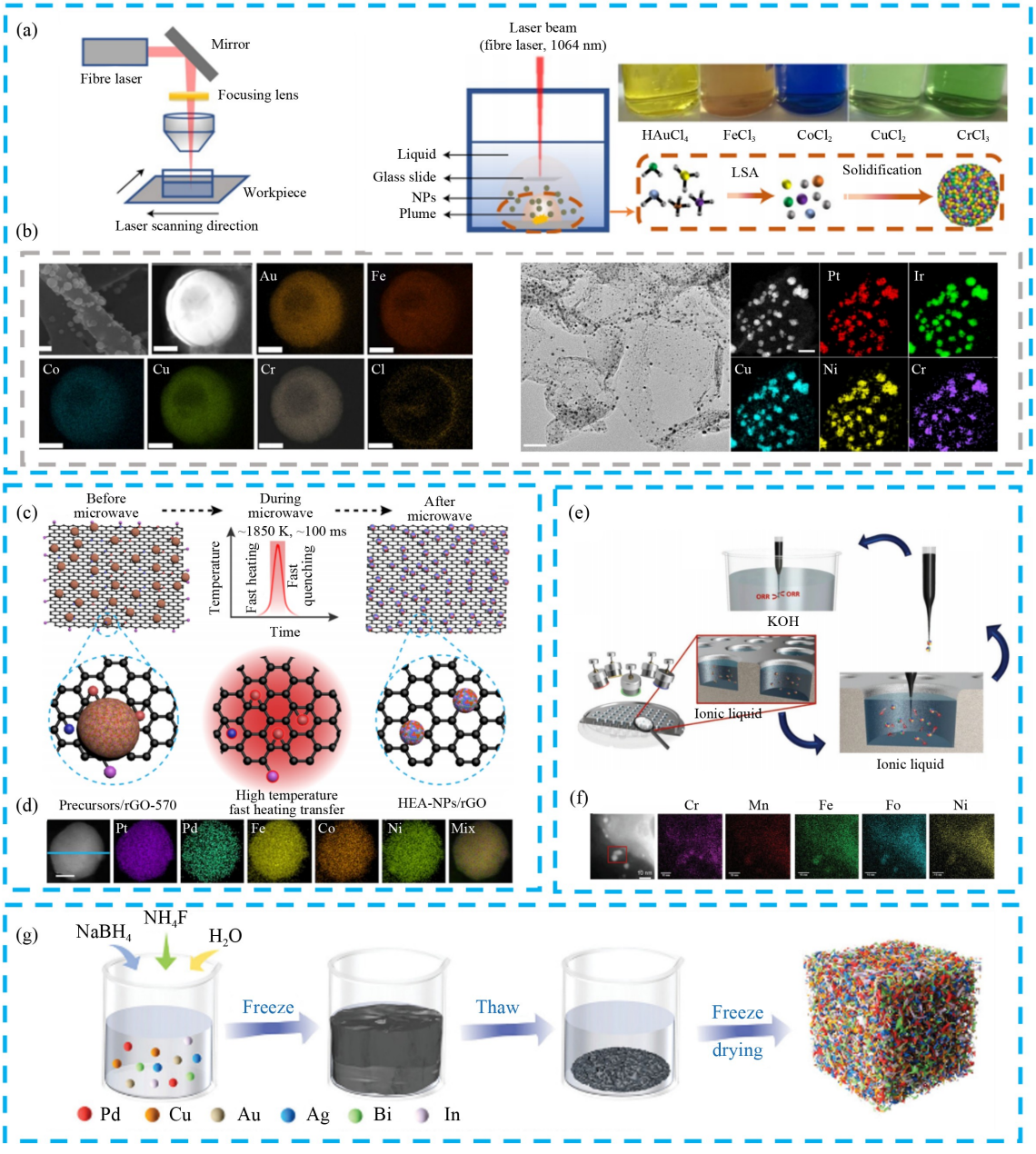

Fig. 7 Other preparation methods of HEAs.

(a) Preparation of AuFeCoCuCr HEA by laser ablation method; (b) SEM and EDS images of AuFeCoCuCr HEA loaded on CNFs (left), elemental mapping images of denary AuFeCoCuCr HEAs (right) (scale bar: 20 nm) (adapted with permission from Wang et al. [79], copyright 2022, Spinger Nature); (c) preparation of HEA by microwave thermal method; (d) EDS images of PtIrCuNiCr HEA on graphene (adapted with permission from Qiao et al. [82], copyright 2021, ACS Publications); (e) preparation of HEA by sputtering deposition; (f) EDS images of HEA nanoparticles (CrMnFeCoNi) (adapted with permission from Löffler et al. [83], copyright 2018, Wiley); (g) preparation of HEAs by freeze-thaw method (adapted with permission from Li et al. [85], copyright 2023, Wiley).

demonstrating the broad applicability of the LSA method. As shown in Fig. 7(b), the PtIrCuNiCr-graphene has a uniform distribution of internal elements and excellent performance in water electrolysis.

The microwave heating method enables rapid and uniform heating, providing precise control over particle size, composition, and structure, which makes it a promising technique for industrial applications [80,81]. Qiao et al. [82] reported a novel microwave heating approach for synthesizing HEA nanoparticles. Graphene oxide, due to its numerous functional group imperfections and efficient microwave absorption, was selected as the model substrate. This method allowed graphene oxide to reach a temperature of approximately 1850 K within a few seconds. Utilizing this rapid heating process, they successfully synthesized PtPdFeCoNi HEA nanoparticles with uniformly mixed elements.

Sputtering deposition, a widely used thin-film deposition technique, involves ion bombardment of a solid target, causing atoms or molecules to detach and form a thin film on a substrate. Löffler et al. [83] developed a co-sputtering strategy, adjusting deposition rates and ionic liquids to prepare amorphous HEA nanoparticles (CrMnFeCoNi) with tunable size and composition (Fig. 7(e)). Similarly, Manjón et al. [84] fabricated CrMnFeCoNi HEA colloidal suspensions with varying sizes and structures by modulating the ion concentration in the sputtering ionic liquid. These colloidal suspensions demonstrated excellent electrochemical ORR performance in a 0.1 mol/L KOH electrolyte.

Li et al. [85] developed high-activity, stable HEA aerogels using a freeze-thaw method. The synthesis process involves several key steps: First, multiple metal salts are dissolved in ultrapure water to form a homogeneous metal ion solution (Fig. 7(g)). Then, ammonium fluoride and sodium phosphine are added to the solution. Next, the solution is rapidly cooled to liquid nitrogen temperature, which causes the water in the solution to freeze rapidly and form a gel. During this freezing process, the metal ions and other chemicals coalesced, forming a preliminary gel-like structure. The gel is subsequently thawed, washed to remove residual impurities, and placed in a freeze dryer for drying. This freeze-drying step removes the moisture from the gel by sublimation at low temperatures, preserving its microstructure.

The key steps in this synthesis method include dissolving metal salts, adding ammonium fluoride and sodium phosphine, rapid cooling with liquid nitrogen, thawing and washing, and freeze-drying. Through these steps, HEA aerogels with multiple metal elements can be effectively synthesized. These aerogels not only possess high surface area and porosity but also allow for optimization of catalytic performance through appropriate metal ratios, making them suitable for applications such as CO_2 reduction.

4 Characterizations

The evolution of HEAs from micron-scale structural materials to nano-scale functional materials has significantly accelerated their development in catalysis. Advanced characterization techniques play a crucial role in unraveling the underlying structures and properties of HEAs. These techniques include detailed analysis of elemental composition, distribution, phase structures, surface chemical states, and lattice distortion effects, along with *in situ* characterization approaches (Fig. 8). By providing in-depth insights into the microstructures and chemical states of HEAs, these methods drive performance optimization and support the development of new applications. They provide a solid foundation for the design and implementation of HEA catalysts in various catalytic systems.

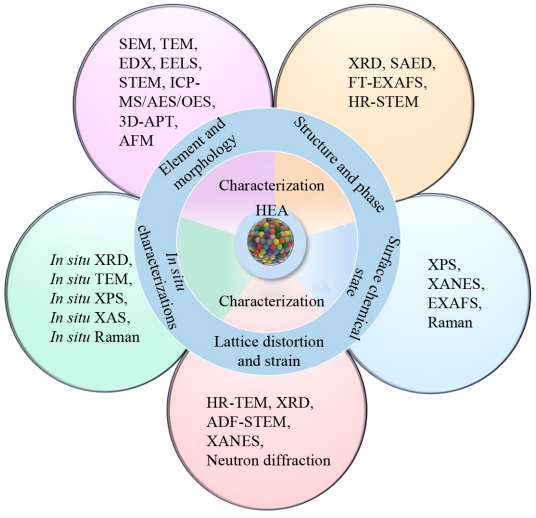

Fig. 8 Different techniques for characterizations of HEAs.

4.1 Elements and forms

HEAs are composed of at least five elements, requiring the precise determination of both the content and distribution of these elements. Advanced elemental and morphological characterization techniques are therefore indispensable in this regard. Inductively coupled plasma (ICP) technology plays a crucial role in the accurate qualitative and quantitative analysis of elemental compositions. ICP techniques are particularly valued for their high sensitivity and broad dynamic range, enabling the precise detection of diverse elemental compositions in HEAs.

Atomic electron tomography (AET) is an advanced three-dimensional atomic structure characterization

technique which accurately reveals the atomic arrangement and structural details inside a material. By imaging and reconstructing the three-dimensional image of the sample from different angles, AET provides insights into the element distribution, interface structure, defects and nanostructures inside HEAs. This is essential for understanding the relationship between microstructure and properties, which is crucial for guiding the design, optimization, and the development of new materials.

Yang et al. [86] pioneered an AET reconstruction method to experimentally determine the three-dimensional atomic positions in high-entropy metallic glass nanoparticles containing eight elements (Co, Ni, Ru, Rh, Pd, Ag, Ir, Pt) for the first time (Figs. 9(a) and 9((b)). Their findings revealed that, although the short-range ordered structures in the amorphous samples were geometrically disordered, when these structures connected, they formed superclusters resembling crystals, exhibiting mid-range order. In these amorphous samples, four crystal-like mid-range ordered structures were identified: face-centered cubic (FCC), hexagonal close packing (HCP), body-centered cubic (BCC), and simple cubic packing (SC), which exhibited translational rather than orientation order (Fig. 9(c)). This work provided direct experimental evidence for the study of the three-dimensional structure of amorphous materials.

Ma et al. [36] demonstrated the uniform distribution of all elemental components in HEAs using three-dimensional atom probe tomography (3D-APT) (Fig. 9(d)). Liu et al. [38]. revealed the 3D atomic structure and surface electronic structure of HEA PdFeCoNiCu (PdM) nanocrystals by using the AET technique. They found significant differences in the chemical order of high entropy intermetallic compound nanocrystals formed at 300 and 500 °C, with low order and high order PdM (M = Fe, Co, Ni, Cu) atomic arrangement structure, respectively. However, the surfaces of both nanoparticles were mainly composed of chemically disordered FCC-PdM solid

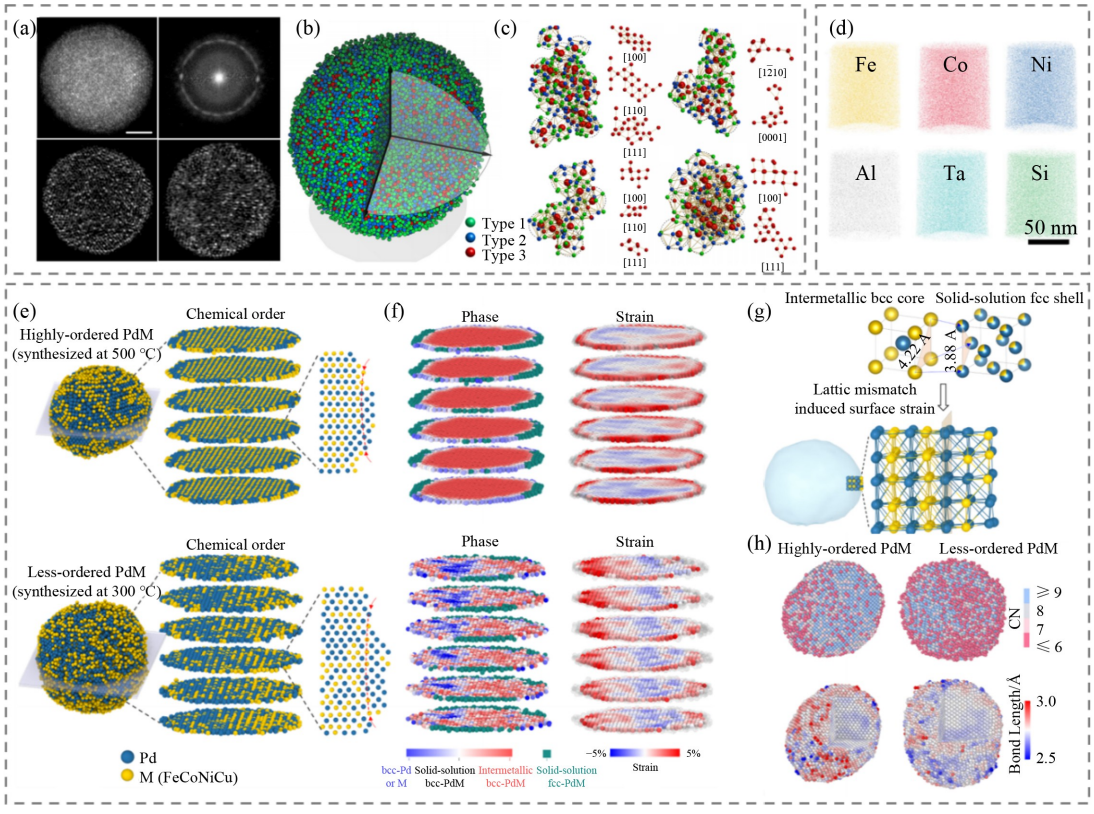

Fig. 9 3D characterization of HEN.

(a) Three-dimensional atomic structure of high-entropy metallic glass nanoparticles accurately determined by AET (representative experimental image (top left), corresponding average two-dimensional power spectrum (top right), 3D reconstructed slices with a thickness of 2.4 microns in the *x*–*y* and *y*–*z* planes (bottom two diagrams) (scale bar: 2 nm); (b) an experimental three-dimensional atomic model of high-entropy metallic glass nanoparticles (adapted with permission from Yang et al. [86], copyright 2021, Springer Nature); (c) four crystal-like intermediate-range ordered structures co-existing in metallic glass nanoparticles; (d) 3D-APT images (adapted with permission from Ma et al. [36], copyright 2024, Springer Nature); (e) layer-by-layer atomic slices (blue: Pd, yellow: Fe, Co, Ni, Cu) of highly ordered and less ordered PdM nanoparticles prepared at 500 and 300 °C; (f) phases and strain diagrams; (g) representative interceptions of the intermediate metal core/solid solution shell interface showing lattice mismatches and shell remodeling; (h) three-dimensional distribution of coordination number (CN) (top) and nearest atom-atom bond length (bottom) of highly ordered and low-ordered PdM nanocrystals (adapted with permission from Liu et al. [38], copyright 2024, ACS Publications).

solutions, with almost no chemically ordered intermetallic compound phase (Figs. 9(e) and 9(f)). The intermetallic compounds with core-shell structures formed a heterostructural interface composed of BCC (nucleus) and FCC (shell) phases near the surface. The surface stress induced by the lattice mismatch between the two leads to the distortion of the near surface lattice.

These three-dimensional atomic structures clearly reveal the origin of near-surface stresses in high entropy intermetallic compounds. Further quantitative analysis of the stress, coordination number, and atomic spacing of the nanocrystals revealed that, despite differences in the internal chemical order of the two types of intermetallic compounds, their near-surface stress distribution, atomic coordination number, and atomic spacing were similar (Figs. 9(g) and 9(h)).

Energy dispersive X-ray spectroscopy (EDX) is often used in conjunction with electron microscope techniques, such as SEM or TEM, to detect characteristic X-rays produced by the interaction between the sample and the electron beam. This provides a fast and accurate elemental map of the near-surface region of HAEs. The resulting data can be used to qualitatively and quantitatively determine the elemental composition and concentration, providing insight into the structure and chemistry of the material. Linear scanning with EDX produces detailed spectra and distribution maps, while comprehensive elemental mapping can be achieved through electron energy loss spectroscopy (EELS). Moreover, EDX combined with scanning transmission electron microscopy (STEM) has become an indispensable tool for high-resolution spatial analysis of elemental distributions in HEAs (Fig. 10(a)) [87]. These atomic-resolution electron microscopy results show that, despite the internal atomic ordering of HEA nanocrystals, the surface atomic configuration remains basically unchanged, and all surfaces exhibit chemically disordered solid solution phases.

4.2 Structure and phase

Powder X-ray diffraction (PXRD) is a widely used

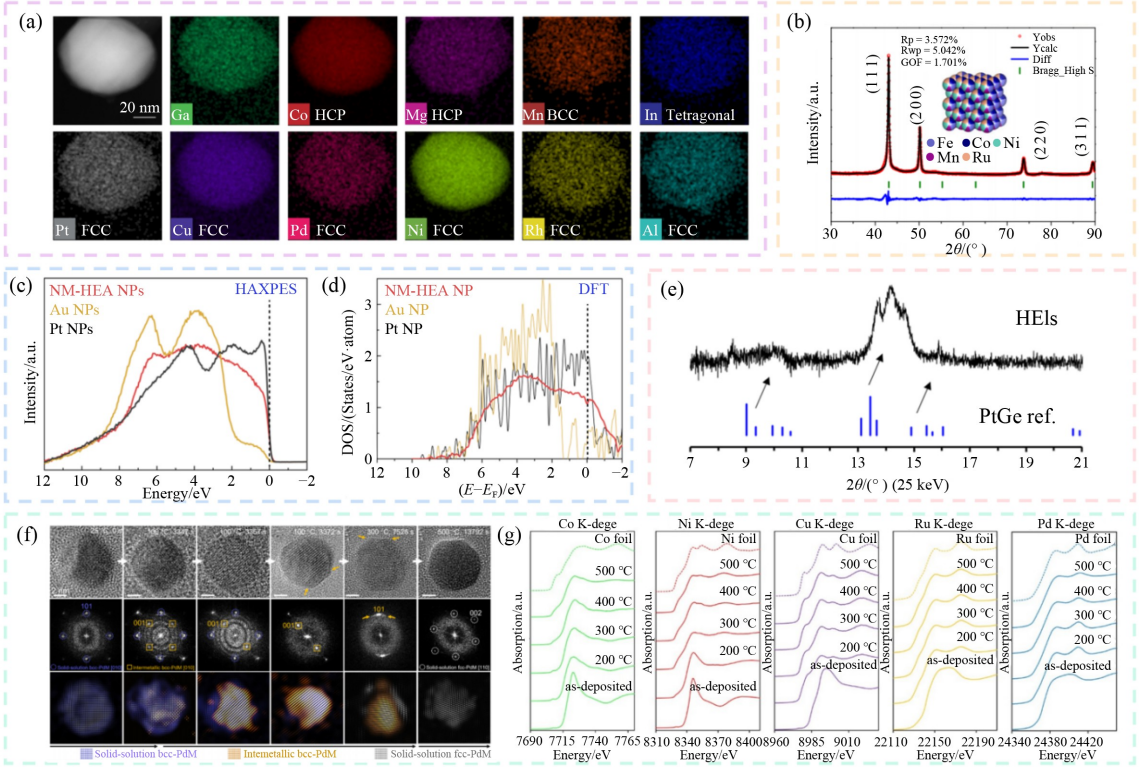

Fig. 10 Various characterization techniques for HEA.

(a) Structural imaging of HAADF-STEM and EDX images of HEA nanoparticles (adapted with permission from Cao et al. [87], copyright 2023, Springer Nature); crystal lattice analysis: (b) structural imaging of PXRD pattern of FeCoNiMnRu HEA nanoparticles (adapted with permission from Hao et al. [88], copyright 2022, Springer Nature); chemical state analysis: (c) structural imaging of valence band spectra obtained via HAXPES; (d) electronic structure of DOS distributions of NM-HEA, Pt, and Au nanoparticles calculated through DFT (adapted with permission from Wu et al. [90], copyright 2022, ACS Publications); (e) advanced structural analysis of synchrotron XRD spectra of HEA nanoparticles (adapted with permission from Nakaya et al. [39], copyright 2022, ACS Publications); (f) phase evolution of *in situ* ETEM images showing the phase evolution of high-entropy PdM under 20-Pa-H_2 (adapted with permission from Liu. [38], copyright 2024, ACS Publications); (g) chemical state dynamics of *in situ* XANES spectra of CoNiCuRuPd/TiO_2 during hydrogen reduction from room temperature (adapted with permission from Mori et al. [76], copyright 2021, Springer Nature).

technique for characterizing the structure of materials. It determines the phase structure, lattice parameters, and grain size of crystals by analyzing the XRD patterns of materials. The analysis of PXRD patterns mainly depends on the location and intensity of diffraction peaks, which is particularly important for phase structure analysis of HEAs and other materials. Ideally, the PXRD pattern of HEAs should exhibit diffraction peaks corresponding to a single-phase solid solution (Fig. 10(b)) [88].

By precisely fitting the diffraction peaks of the PXRD data, it is possible to conduct in-depth analyses of the microstructure of the material, including particle size, lattice geometric parameters, and degree of crystallization. This process involves a quantitative analysis of the diffraction peak width and shape to reveal the microscopic features inside the material.

The Fourier transform extended X-ray absorption fine structure (FT-EXAFS) technique is another powerful analytical tool to study local structural changes in metal-metal bonds in alloys and is often used in HEAs applications to demonstrate alloy phase formation and atomic-level bonding interactions [89].

Moreover, high-resolution scanning transmission electron microscopy (HR-STEM) can be used to identify the planar structure of crystals at the atomic scale. Given the complexity of HEAs, fully revealing their crystal structure with a single characterization method can be challenging. Hence, utilizing multiple analytical techniques is essential for confirming whether the synthesized materials qualify meet the criteria of HEAs.

4.3 Surface chemical state

Electrocatalytic reactions usually occur on the surface of the catalyst and the interface of the electrolyte. As such the chemical state of the surface of the electrocatalyst often determines the reaction mechanism of electrocatalysis. X-ray Photoelectron Spectroscopy (XPS) is a widely used surface analysis technique that allows for the examination of elemental composition and chemical states of materials. However, its high surface sensitivity limits its analysis only the outer few nanometers of the surface of a material.

X-ray absorption spectroscopy (XAS), which includes X-ray absorption near-side structure (XANES) and extended X-ray absorption fine structure (EXAFS), is another powerful tool for analyzing the chemical state and local coordination environment of elements at the surface of materials. In the study of HEAs, XAS provides crucial information about valence states, coordination atoms, coordination and bond lengths of elements. Specifically, XANES is primarily employed to investigate the valence states of elements, while EXAFS reveals local atomic structural characteristics, including the type, number, distance, and relative arrangement of neighboring atoms.

Hard X-ray photoelectron spectroscopy (HAXPES) can further reveal the electronic structure of HEAs catalyst, offering insights into the multi-element synergism in these materials. Wu et al. [90] used HAXPES and density functional theory (DFT) simulations to study the precious metal HEA (RuRhPdAgOsIrPtAu). The data revealed characteristic peaks in the valence bond spectrum for the HEA nanoparticles, while the single metals (e.g., Au and Pt) showed distinct characteristic peak in the valence band spectrum (Fig. 10(c)). The DFT simulation results (Fig. 10(d)) also confirmed that HEA nanoparticles exhibit a smoother density of states (DOS) distribution than single metals, with no distinct peaks in the valence band spectrum. This smooth distribution is attributed to the rich atomic configuration and low-level degeneracy in HEAs. In contrast, most mono-metals exhibit a similar state density distribution due to their atomic uniformity. This observation suggests that in HEAs, each atom loses its original identity as an element and instead plays an integral role as part of the whole. By adjusting the states of adjacent atoms, an ideal local DOS can be created to favors electrocatalytic reactions, thereby enhancing catalyst performance [90].

4.4 Lattice distortion

Due to the atomic radii differences and irregular arrangements, HEAs often experience lattice distortion and deformation, which can significantly affect their practical performance in catalytic reactions. Therefore, studying these lattice distortions and deformations in HEAs is of critical importance for optimizing HEA-based catalysts. However, accurately characterizing these lattice distortions is a highly challenging task that requires a combination of multiple advanced characterization techniques.

Commonly employed techniques include XRD, which is used to analyze lattice distortion in HEAs; TEM, which allows for observing local structural changes and distortions in the alloy; electron backscatter diffraction (EBSD), which is useful for identifying structural anomalies in HEAs; and atomic force microscopy (AFM), which probes surface defects at the nanoscale. These characterization methods provide valuable insights into the lattice distortions and damage in HEAs, offering pathways for optimizing their catalytic performance.

For instance, Fig. 10(e) presents the XRD pattern of an HEA catalyst. Unlike FCC or HCP HEAs, the diffraction peaks of this HEA exhibit a slight redshift compared to those of the PtGe precursor. This shift can be attributed to lattice contraction caused by smaller elements, such as Co and Cu, in substitution of Pt atoms in the lattice [39].

4.5 *In situ* characterization

In situ characterization techniques play a pivotal role in

the study of HEA catalysts by enabling real-time observation of dynamic changes during both the preparation process and actual application [91]. These techniques allow for the assessment and analysis of changes in catalyst structure, surface states, and chemical properties, which are crucial for optimizing catalytic performance, enhancing stability, and revealing reaction mechanisms. As a complement to traditional characterization methods, *in situ* techniques are essential for establishing detailed structure-performance relationships in HEAs, significantly advancing the field.

Liu et al. [38] utilized *in situ* environmental transmission electron microscopy (ETEM) to investigate the transformation of the disordered BCC solid solution structure of a PdFeCoNiCu HEA (denoted as PdM) into an ordered intermetallic compound (Fig. 10(f)). TEM imaging and corresponding fast Fourier transform (FFT) analysis revealed that the initial PdM nanoparticles exhibited BCC solid solution characteristics along the (010) crystal plane. Between 3347–3372 s at 100 °C, the BCC-PdM solid solution gradually transformed into an ordered intermetallic BCC-PdM, with a 3 nm lattice spacing observed exclusively on the (001) crystal plane of the intermetallic PdM. Surface analysis of the intermetallic PdM revealed depressions on the (001) and (101) planes, along with curved diffraction points (indicated by arrows), suggesting strain on the HEA surface. As the temperature increased further to 300–500 °C, the intermetallic BCC-PdM gradually reverted to the FCC-PdM solid solution, accompanied by the disappearance of surface strain and curvature, demonstrating the significant impact of temperature on the microstructural regulation of HEAs.

In situ X-ray absorption spectroscopy (XAS) has been widely applied in electrochemical reactions involving gases, particularly to study the coordination structure of electrode materials [92]. Similarly, Mori et al. [76] employed *in situ* X-ray absorption near-edge structure (XANES) techniques to analyze the reduction process of the precursors of CoNiCuRuPd HEA nanoparticles under high-temperature hydrogen atmospheres, revealing the reduction sequence (Fig. 10(g)). The study showed that all precursors began to reduce at 200 °C, and by 400 °C, the XANES spectra of all elements aligned with those of their corresponding metal foils, confirming the complete conversion of all elements to their metallic states at this temperature.

5 Electrocatalytic reduction reaction applications

The application of HEAs in electrocatalysis is emerging as a prominent research hotspot, particularly in the context of energy conversion. Due to their unique composition and structure, HEAs demonstrate significant potential in a range of electrocatalytic reactions. This review focuses on the applications of HEAs in three key areas of electrocatalysis: the ORR, the HER, and the CO_2RR.

5.1 ORR

ORR is a critical electrochemical process in clean energy devices, where oxygen is reduced to water or hydrogen peroxide, with its efficiency directly determining the energy conversion rate and overall performance of the device [93–96]. HEAs have gained substantial attention due to their exceptional electrocatalytic properties, making them promising candidates for improving ORR efficiency [97].

Wang et al. [98] developed a carbon-supported PtFeCoNiMn HEA catalyst (PtFeCoNiMn/OMC), as shown in Fig. 11(a). This catalyst exhibited exceptional ORR performance in acidic media, with a half-wave potential ($E_{1/2}$) of 0.88 V (versus RHE) and a mass activity of 1.12 A/mg$_{Pd}$, significantly outperforming commercial Pt/C catalysts (0.86 V, 0.30 A/mg$_{Pd}$) (Fig. 11(b)). These results indicate Pt in PtFeCoNiMn/OMC exhibits notably higher intrinsic activity compared to Pt/C. Additionally, the catalyst demonstrated remarkable durability, with only a 20-mV negative shift in $E_{1/2}$ after 30000 cyclic voltammetry (CV) cycles. This enhanced stability is attributed to the strong electronic interactions among the multiple components, which effectively inhibit the oxidation and dissolution of surface-active metal atoms. Theoretical calculations further revealed significant differences in oxygen binding energies at the Pt sites within the HEA compared to pure Pt. For pure Pt, the rate-determining step in the ORR is the transition from *O to *OH, exhibiting a free energy change no less than 0.3 eV. In contrast, the PtFeCoNiMn HEA exhibited a minimum free energy change of 0.7 eV, which exceeds that of pure Pt (Fig. 11(c)). This larger free energy change suggests improved ORR kinetics for PtFeCoNiMn HEA in ORR.

Zuo et al. [99] deloped a hollow nanospheres HEA on RGO$_3$-CNTs (PdCuMoNiCo NHSs), as shown in Figs. 11(d) and 11(e). PdCuMoNiCo NHSs ($E_{1/2}$ = 0.86 V) showed similar performance comparable to that of Pt/C in ORR electrochemical test of acid media. Notably, the catalytic activity of PdCuMoNiCo NHSs (mass activity of 0.882 A/mg$_{Pd}$) far exceeded that of PdCuMoNiCo NPs (0.149 A/mg$_{Pd}$). This enhanced performance is attributed to the hollow structure of the catalyst, which increases the catalytic active surface area.

Zhao et al. [100] developed a catalyst supported on a carbon substrate (N–Pt/HEA/C), featuring a PtCoFeNiCu HEA core and a shell with abundant platinum, as depicted in Fig. 11(h). In 0.1 mol/L $HClO_4$ medium, N–Pt/HEA/C exhibited superior ORR performance with

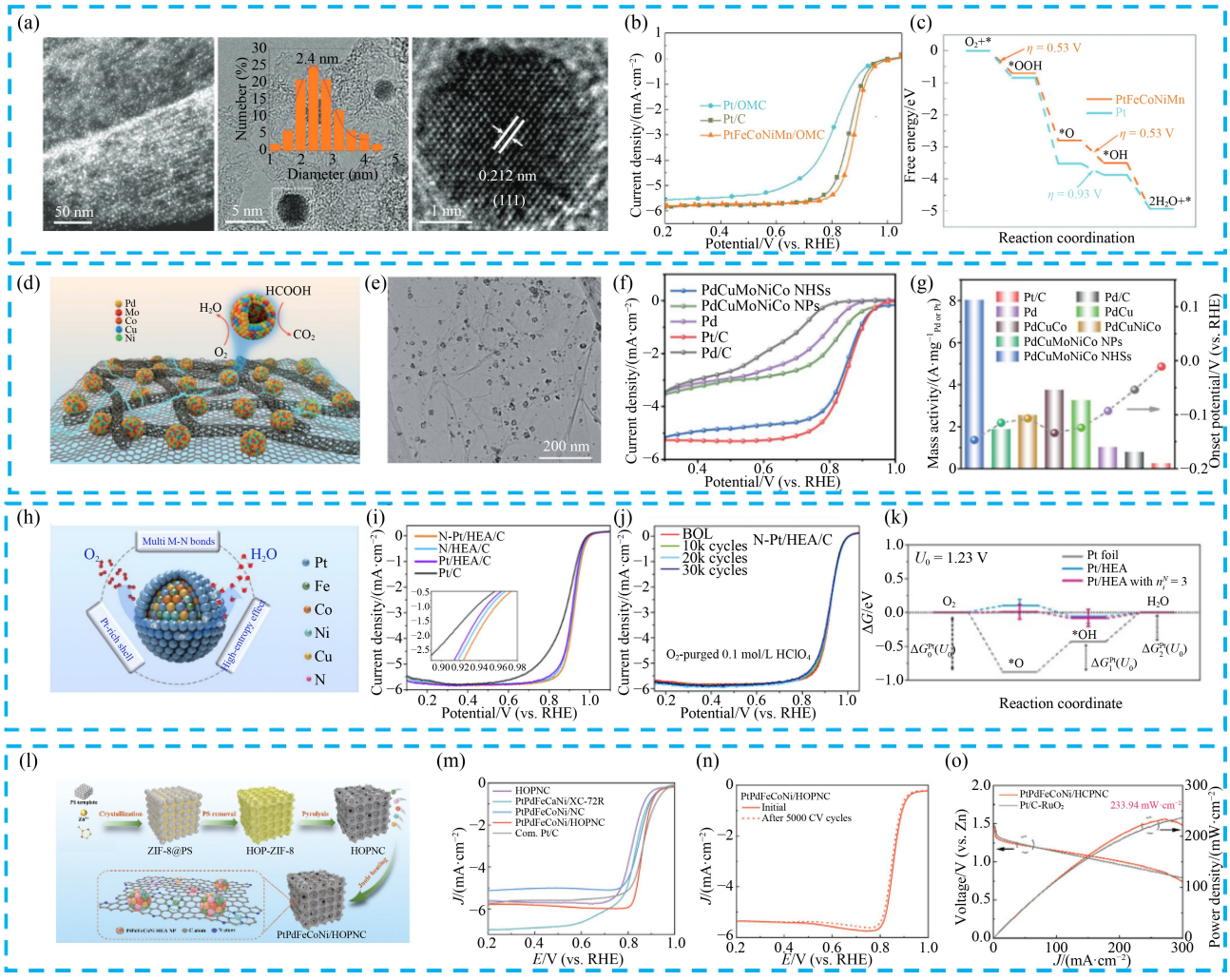

Fig. 11 ORR performances of HEAs.

(a) HAADF-STEM image (left) and TEM images (middle and right) of PtFeCoNiMn/OMC; (b) LSV curves of PtFeCoNiMn/OMC in 0.1 mol/L $HClO_4$; (c) Gibbs free energy diagrams of monometallic Pt and PtFeCoNiMn HEA (adapted with permission from Wang et al. [98], copyright 2024, Wiley); (d) schematic illustration of PdCuMoNiCo NHSs/RGO_3-CNT; (e) TEM image of PdCuMoNiCo NHSs/RGO_3-CNT; (f) LSV curves of PdCuMoNiCo NHSs/RGO_3-CNT; (g) comparison of onset potential and mass activity (adapted with permission from Zuo et al. [99], copyright 2022, RSC Publishing); (h) schematic of N–Pt/HEA/C; (i) LSV curves of N–Pt/HEA/C; (j) stability tests of N–Pt/HEA/C; (k) Gibbs free energy diagrams of N–Pt/HEA/C, Pt/HEA, and Pt foil (adapted with permission from Zhao et al. [100], copyright 2024, ACS Publications); (l) synthesis process of PtPdFeCoNi/HOPNC; (m) LSV curves of PtPdFeCoNi/HOPNC in 0.1 mol/L KOH; (n) stability tests of PtPdFeCoNi/HOPNC;(o) zinc-air battery performance of PtPdFeCoNi/HOPNC (adapted with permission from Xie et al. [101], copyright 2024, Wiley).

an $E_{1/2}$ of 0.92 V. This value surpassed those of N-HEA/C (0.91 V), Pt/HEA/C (0.91 V), and Pt/C (0.88 V), as shown in Fig. 11(i). Durability tests, depicted in Fig. 11(j), revealed that after 30000 cycles of triangular wave potential, the $E_{1/2}$ of N–Pt/HEA/C declined by only 8 mV, demonstrating exceptional stability. The high-entropy structure of the Pt-rich surface optimizes *O and *OH adsorption energies, facilitates efficient electron transfer, and significantly mitigates *OH poisoning. As illustrated in Fig. 11(k), the free energy of *O adsorption on Pt/HEA and N–Pt/HEA surfaces is markedly lower than that on Pt foil, promoting improved ORR activity. Furthermore, the weaker *OH adsorption on N–Pt/HEA and Pt/HEA diminishes *OH poisoning compared to Pt, thereby enhancing long-term activity and durability. These combined features make N–Pt/HEA/C a highly effective catalyst with outstanding ORR performance and stability.

Xie et al. [101] successfully synthesized highly dispersed PtPdFeCoNi HEA nanoparticles with a size of just 2 nm, using an ultrafast Joule heating method. These nanoparticles were randomly distributed as multi-metallic single atoms within a porous nitrogen-doped carbon framework (PtPdFeCoNi/HOPNC), as shown in Figs. 11(l)–11(n). The synthesized catalyst's ORR performance was evaluated in O_2-saturated 0.1 mol/L KOH

solution. The $E_{1/2}$ of PtPdFeCoNi/HOPNC was 0.866 V, comparable to that of commercial Pt/C. Remarkably, the kinetic current density (J_k) of PtPdFeCoNi/HOPNC at 0.85 V reached 13.89 mA/cm^2, significantly surpassing that of commercial Pt/C (11.20 mA/cm^2). This improvement is primarily attributed to the hierarchical porous structure, which enhances mass transport during the ORR process. In durability tests, after 5000 CV cycles, the $E_{1/2}$ of PtPdFeCoNi/HOPNC remained nearly unchanged, demonstrating excellent stability. Additionally, a quasi-solid-state zinc-air battery (ZAB) was assembled using PtPdFeCoNi/HOPNC as the air cathode catalyst and a transparent, robust hydrogel as the electrolyte. The ZAB achieved a peak power density of 233.94 mW/cm^2, indicating its excellent performance in energy devices, as shown in Fig. 11(o).

5.2 HER

HER is a clean, environmentally friendly, and cost-intensive technique for producing clean, high-energy-density hydrogen fuel. It provides an effective solution for converting and storing intermittent energy sources, addressing the growing global energy demands while mitigating environmental issues [102,103]. To date, Pt-based nanomaterials, have remained the most widely utilized electrocatalysts for HER due to their optimal hydrogen binding strength at the initial bond level [104,105]. However, the widespread application of platinum in electrolytic cells is significantly limited by its high cost, limited electrochemical durability, and decreased catalytic activity over time [106]. In this context, alloying has emerged as a promising strategy to overcome these limitations, involving both non-Pt and Pt-based alloys. This approach reduces the use of precious metals while improving electrocatalytic activity, thereby offering a feasible pathway for the widespread application of HER technologies [107].

For Pt-based HEAs, Li et. al. [108] reported a pentanary PdRhMoFeMn HEA catalyst. EDS mapping demonstrated the uniform elemental dispersion within the PdRhMoFeMn HEA, as shown in Fig. 12(a). The catalyst exhibited outstanding HER performance, with overpotentials at a current density of 10 mA/cm^2 (η_{10}) of 6, 23, and 26 mV under acidic, neutral, and alkaline conditions, respectively, all outperforming Pt/C catalysts (Figs. 12(b)

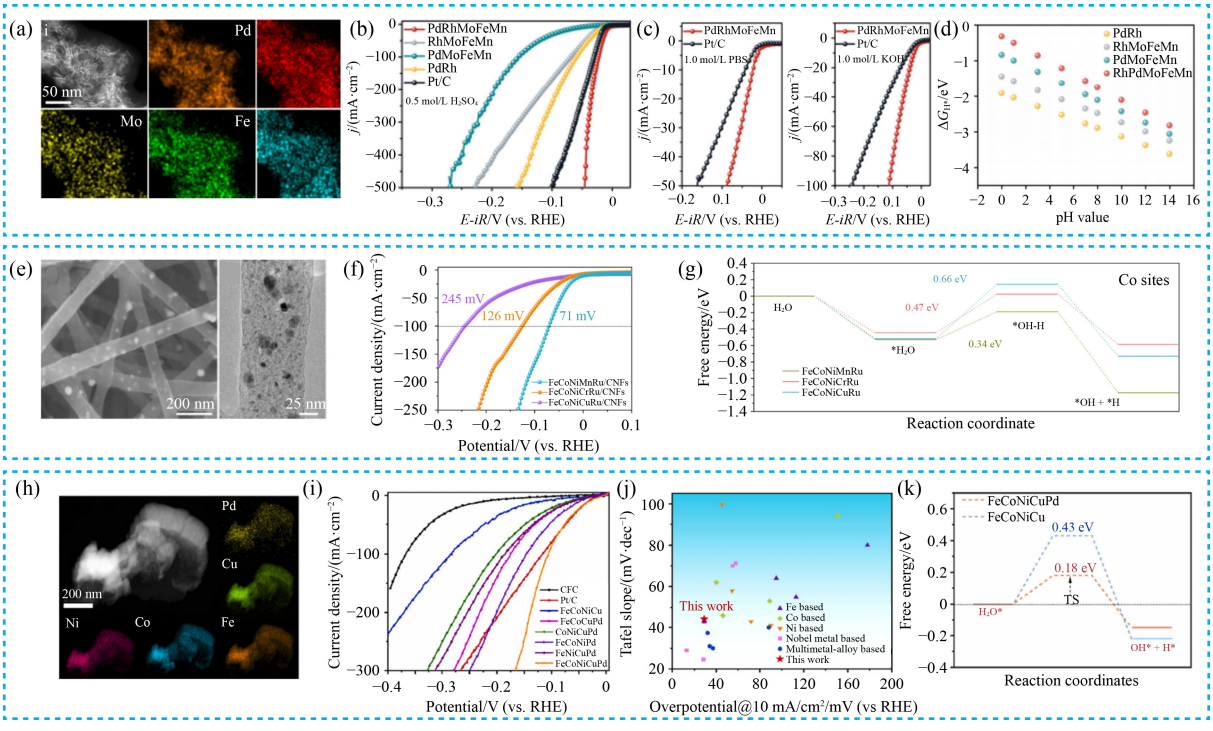

Fig. 12 Applications of non-Pt HEAs in HER.

(a) HAADF-STEM and EDS of PdRhMoFeMn HEA; (b) LSV of PdRhMoFeMn HEA at 0.5 mol/L H_2SO_4; (c) LSV of PdRhMoFeMn HEA at 1 mol/L PBS and 1 mol/L KOH; (d) relationship between the free energy and pH of PdRhMoFeMn HEN (adapted with permission from Li. [108], copyright 2024, Springer Nature); (e) FE-SEM (left) and TEM (right) images of FeCoNiMnRu/CNFs; (f) HER polarization curves of FeCoNiXRu/CNFs (X = Mn, Cr, Cu); (g) reaction energy distribution for water dissociation at Co sites on the surfaces of HEA (adapted with permission from Hao et al. [88], copyright 2022, Springer Nature); (h) HAADF-STEM and EDS of FeCoNiCuPd HEA; (i) HER polarization curve of FeCoNiCuPd HEA; (j) comparison of the HER performance between the FeCoNiCuPd HEA and other catalysts; (k) free energy diagram of FeCoNiCuPd HEA (adapted with permission from Wang et al. [109], copyright 2022, Elsevier).

and 12(c)). Theoretical calculations revealed that the Rh sites in PdRhMoFeMn possess the lowest Gibbs free energy of hydrogen adsorption (ΔG_{H*}), confirming Rh as the primary active site for HER in acidic media. Over a wide pH range, the ΔG_{H*} of PdRhMoFeMn approached the optimal value of 0 eV, significantly lower than that of PdRh, indicating that the synergistic effects of multiple elements contribute additional catalytic activity (Fig. 12(d)). DOS analysis showed that the d-band center of Rh in PdRhMoFeMn (−1.95 eV) is further from the Fermi level than in PdRh (−1.43 eV) and RhMoFeMn (−1.68 eV). Additionally, the integrated crystal orbital Hamilton population (ICOHP) value for PdRhMoFeMn (−0.89 eV) was higher than those for RhMoFeMn and PdRh. These findings indicate that the high-entropy structure effectively weakens the metal-hydrogen adsorption bonds in Pd, Mo, Fe, and Mn, thereby enhancing hydrogen adsorption and desorption.

Hao et al. [88] proposed various HEA systems of FeCoNiXRu (X: Cu, Cr, Mn) and loaded them onto carbon nanofibers (CNF) (Fig. 12(e)). They discovered that introducing different electronegative elements into the HEA led to substantial charge rearrangement, forming Co and Ru catalytic sites capable of stabilizing both OH and H intermediates, which significantly improved the performance of water electrolysis. As shown in Fig. 12(f), electrochemical tests demonstrated that FeCoNiMnRu/CNF exhibited the best HER performance, achieving the lowest overpotential (η_{100}) of 71 mV and a Tafel slope of 67.4 mV/dec. DFT calculations showed that the formation and adsorption of H and OH intermediates from water dissociation were the potential-determining steps (PDS) that control the rate of hydrolysis dissociation. To identify the active centers, the adsorption energies of different metal sites in FeCoNiMnRu were calculated. The Co site in FeCoNiMnRu was found to be the active center for H_2O dissociation, while the Ru site served as the active center for H adsorption. Additionally, the adsorption energies of H* and OH* dissociated from H_2O at the Co and Ru sites in FeCoNiXRu (X = Cu, Cr, Mn) were tested. The results revealed that the adsorption energy of H* and OH* at the Co site in FeCoNiMnRu was the lowest, at just 0.34 eV. Similarly, the H* adsorption energy at the Ru site in FeCoNiMnRu was also the lowest, at −0.07 eV (Fig. 12(g)). These findings indicate that introducing Mn, with its low electronegativity, significantly lowered the energy barrier of H_2O dissociation at the Co and Ru sites, thus optimizing the kinetic performance of the HER reaction.

Wang et al. [109] prepared an FeCoNiCuPdC HEA thin film catalyst, which was deposited on carbon fiber cloth (CFC) through the magnetron sputtering method. HAADF-STEM and EDS analysis confirmed the uniform distribution of various metals (Fig. 12(h)). As shown in Figs. 12(i) and 12(j), in a 1 mol/L KOH electrolyte, this catalyst exhibited excellent hydrogen evolution reaction (HER) performance. The overpotential of FeCoNiCuPd/CFC at 10 mA/cm^2 was only 29 mV, and the Tafel slope was 47.2 mV/dec, superior to that of Pt/C (35.4 mV, 44.3 mV/dec). To explore the reason for the excellent HER activity, DFT calculations were employed to study the electronic structure of FeCoNiCuPd and the adsorption free energy of reaction intermediates at all possible active sites on the (111) surface. The results showed that the synergistic effect of various metal sites effectively regulates the electronic structure, reduces the energy barrier of hydrolysis, and enhances charge transfer. Additionally, the interaction among multiple metallic elements adjusted the d-band center of the surface adsorption sites, promoting hydrogen adsorption/desorption and reducing the Gibbs free energy (ΔG_{H*}), thus ultimately achieving high-efficiency HER activity (Fig. 12(k)).

In Pt-based HEAs, Zhao et al. [110] reported PtRuMoFeCoNi HEA quantum dots (HEA-QDs), which are nanometer-scale particles composed of multiple elements distributed randomly, as shown in Fig. 13(a). This high-entropy structure enhances synergistic interactions among the elements. The study demonstrated that HE-QDs significantly enhanced HER kinetics across various pH conditions (acidic, neutral, and basic). The catalysts showed low overpotential, fast reaction rates, and high current densities, as shown in Figs. 13(b) and 13(c). Moreover, the HEA-QDs exhibited excellent stability, with current remaining nearly unchanged after 10000 CV cycles. Theoretical calculations indicated that the strong electron transfer from Fe/Co/Ni/Mo to Pt/Ru weakened the free energy of adsorbed hydrogen, thereby improving reactivity, as shown in Fig. 13(d). Advanced analyses revealed that the synergistic effects in HE-QDs arised from their electronic properties, lattice distortion, and surface states.

Kang et al. [111] reported a core-shell structured PtPdRhRuCu mesoporous nanosphere (PtPdRhRuCu MMN) with tunable composition and an exposed porous architecture enriched with HEA sites (Fig. 13(e)). Electrochemical tests demonstrated that PtPdRhRuCu MMNs exhibited exceptional electrocatalytic HER activity. In alkaline, acidic, and neutral electrolytes, the PtPdRhRuCu MMNs achieved η_{10} as low as 10, 13, and 28 mV, respectively (Fig. 13(f)). Durability test results showed that the current remained nearly unchanged across an exceptionally wide current density range over 100 h of continuous operation (Fig. 13(g)). The outstanding HER performance is attributed to the synergistic effects between different metal sites and the mesoporous structure, where the electronic interactions between the metals, the high surface area, and porosity of the mesopores, along with efficient electron transport through the interconnected porous network, collectively enhance the conductivity, ensuring superior mass transfer

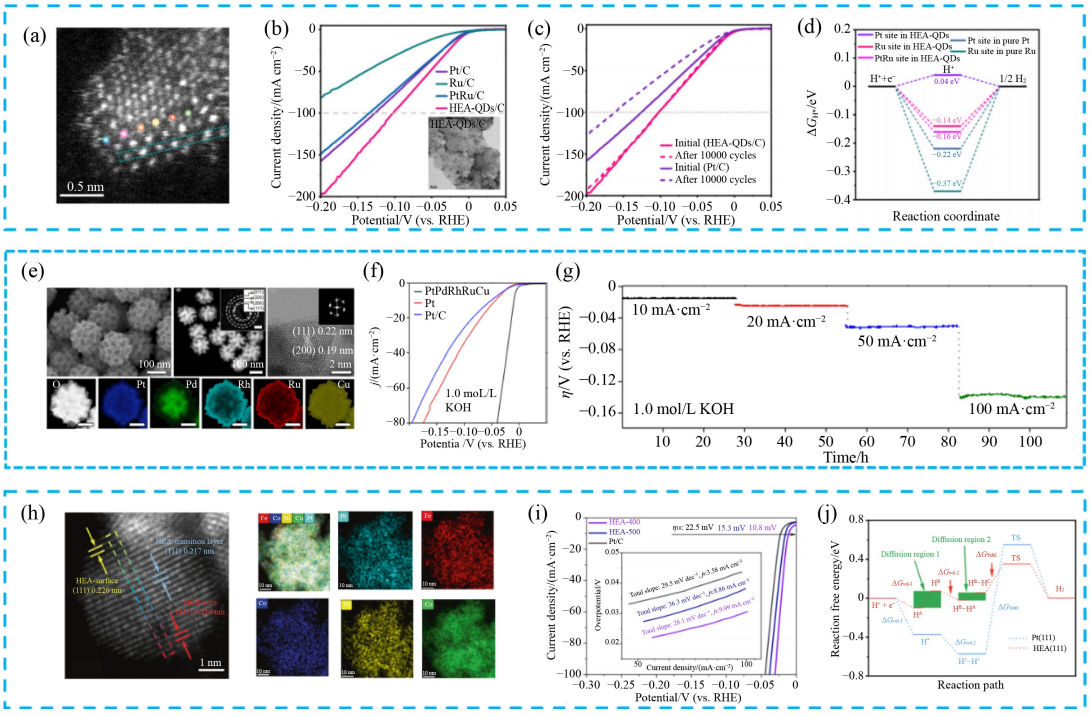

Fig. 13 Applications of Pt-based HEAs in HER.

(a) STEM image of HEA quantum dots (HEA-QD); (b) HER polarization curves of HEA-QD; (c) LSV curves of HEA-QD after 10000 CV cycles; (d) calculated hydrogen adsorption free energy curves for Pt/Ru sites (adapted with permission from Zhao et al. [110], copyright 2024, RSC Publishing); (e) TEM images of PtPdRuRhCu MMN; (f) LSV of PtPdRuRhCu MMN at 1 mol/L KOH; (g) stability tests for different current densities (adapted with permission from Kang et al. [111], copyright 2023, Springer Nature); (h) HAADF-STEM and HAADF-EDS images of HEA-400; (i) polarization curves of HEA-400, HEA-500 (based on different annealing temperatures (400 and 500 °C)); (j) Volmer-Tafel mechanism for HER on HEA (adapted with permission from Chen et al. [112], copyright 2024, Springer Nature).

and electronic conductivity.

Chen et al. [112] designed a PtFeCoNiCu HEA catalyst (HEA-400) (Fig. 13(h)), which demonstrated outstanding catalytic performance for HER, achieving an exceptionally low overpotential of 10.8 mV (η_{10}). Moreover, its intrinsic catalytic activity was almost 5 times higher than that of the benchmark Pt/C, underscoring its potential as a superior alternative for HER applications (Fig. 13(i)). These quantum dots facilitate strong interfacial electron transfer, enabling the efficient flow of electrons between the catalyst and the reactants. This characteristic significantly accelerated the kinetics of HER, consequently boosting the overall hydrogen evolution efficiency (Fig. 13(j)).

5.3 CO_2RR

Table 2 summarizes the high entropy catalyst for CO_2RR.

The CO_2RR, which enables the conversion of CO_2 into products such as hydrocarbons and hydrocarbon oxidation compounds, has become a prominent area of research in the context of HEAs [117,118]. This process not only addresses the growing demand for renewable energy but also mitigates numerous environmental challenges posed by CO_2 emissions. However, CO_2RR is inherently complex, involving a series of proton-electron coupled processes, especially when producing more intricate C_2 and C_{3+} products, making the reaction mechanism more challenging to decipher, and the kinetics of the reaction significantly slower [119,120]. HEAs have garnered widespread attention due to their unique surface sites and specific adsorption properties for reaction intermediates, which can facilitate the CO_2RR process [121–123].

The complex composition and vast design space of HEAs pose challenges to the advancement of their application research. Nevertheless, researchers have explored various approaches, such as theoretical calculation to drive the application of HEAs in CO_2RR. Pedersen et al. [123] combined DFT calculations with ML to identify two promising HEAs. Figure 14(a) shows a schematic of the CO_2RR and CORR. Their calculations predicted the binding energies of various intermediates on the surface of CoCuGaNiZn and AgAuCuPdPt HEA (Fig. 14(b)). They found that lower hydrogen binding energies and higher CO binding energies are beneficial for improving the reaction selectivity. Additionally, the optimal combination of binding energies can be identified by tuning the composition of HEAs, facilitating the prediction and enhancement of HEA performance and

Table 2 High entropy catalyst for CO_2RR

Composition	Synthesis	Electrolyte	Electrochemical performance	Ref.
AgAuCuPdPt	Ball milling	0.5 mol/L K_2SO_4	Complete 100% conversion of CO_2 to gaseous products at a low voltage (−0.3 V vs. RHE), −13.81 mA/cm^2 (at −0.9 V).	Nellaiappan et al. [113]
PdCuAuBiIn	Freeze-thaw method	0.5 mol/L $KHCO_3$	HCOOH and C_1 production achieving Faradaic efficiency (FE) of C_1 products almost 100% from −0.7 to −1.1 V vs. RHE and a maximum FE of HCOOH value of 98.1% at −1.1V vs. RHE	Li et al. [85]
BiInSnSbCdO	CTS method	0.5 mol/L $KHCO_3$	Faradaic efficiency for formate production exceeding 95% across a wide potential window (− 0.5 to −1.6 V) vs. RHE	Cai et al. [114]
$(MoWVNbTa)S_2$	Equilibrium pyrolysis method	1 mol/L KOH	CO Faraday efficiency is higher than 92% at a potential of −0.16 to −0.31 V vs RHE. FE_{CO} = 72% at potential of −0.76 V vs. RHE. At − 0.8 V vs. RHE, the current density reaches 510 mA/cm^2	Cavin et al. [115]
$La(FeCuMnMgTi)O_3$	Ball milling and pyrolysis	0.1 mol/L $NaHCO_3$	Under the condition of constant potential electrolysis (−0.75 V vs. SCE), the total Faraday efficiency (FE) reached 92.5%, among which methyl isopropyl ketone (MIPK, $C_5H_{10}O$) accounted for 54.04%, tert-amyl alcohol (TTA, $C_5H_{12}O$) accounted for 21.19%, and the total FE of C_2^+ products exceeded 70%	Ostovari Moghaddam et al. [116]

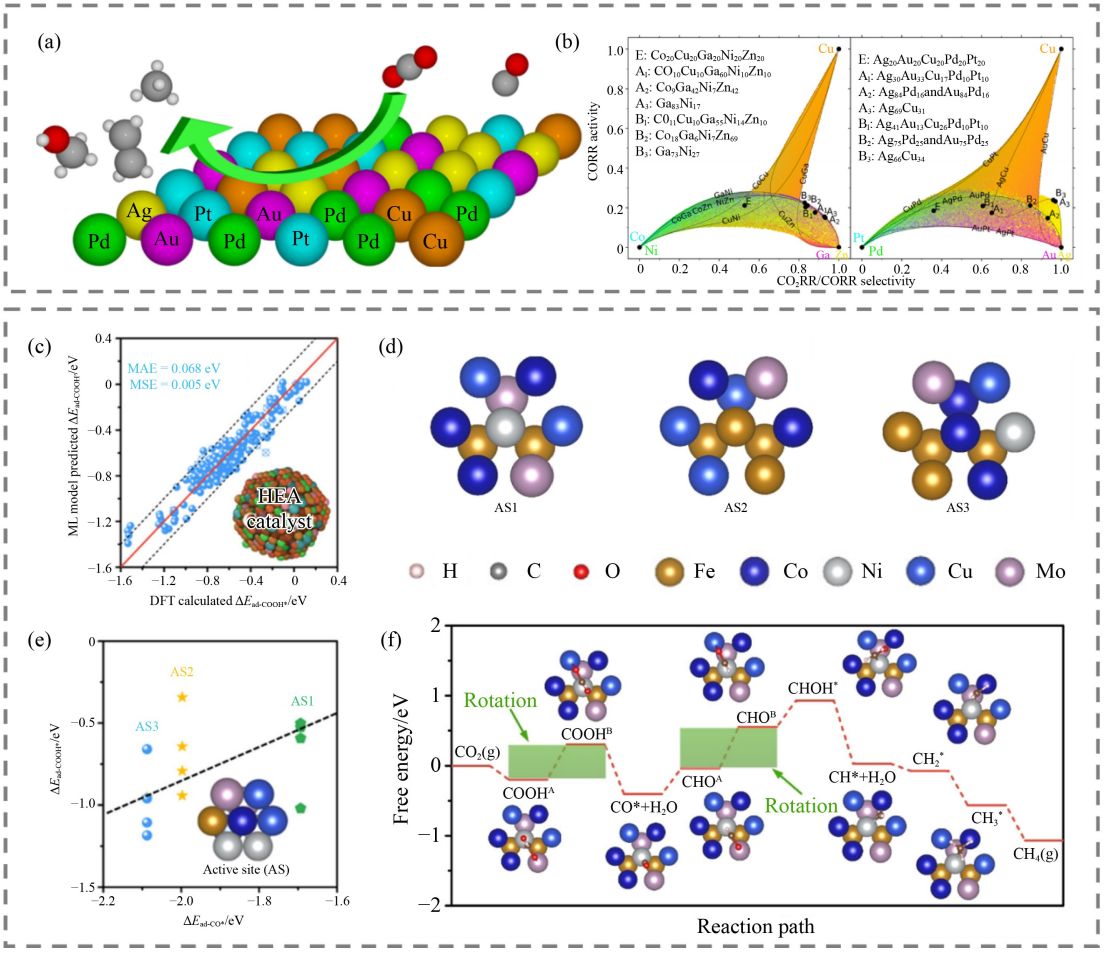

Fig. 14 Theoretical calculation facilitates the application of HEA in CO_2RR.

(a) Schematic representation of CO_2 and CO reduction reactions on HEA catalysts (the red ball representing O, the white ball representing H, and the gray ball representing C); (b) CO_2RR selectivity and activity in the compositional space of CoCuGaNiZn and AgAuCuPdPt HEAs (adapted with permission from Pedersen et al. [123], copyright 2020, ACS Publications); (c) machine learning (ML) predicting the relationship between COOH intermediates of HEA and adsorption energy calculated by DFT; (d) three active site models for HEA (FeCoNiCuMo) (AS1−AS3); (e) relationship between adsorption energies of COOH intermediates and CO intermediates at three active sites (AS1−AS3); (f) reaction process of CO_2RR on AS1, including eight proton−electron transfer processes and two rotation regions (adapted with permission from Chen et al. [124], copyright 2022, ACS Publications).

efficiency. This model provides a method for optimizing disordered alloy compositions to achieve optimal catalytic performance.

Chen et al. [124] made a breakthrough in overcoming scaling relationships for adsorption energies in CO_2RR by employing -guided HEA design, achieving an ultralow limiting potential of 0.29 V. By using a neural evolutionary structure (NES) approach, they generated 200 surface configurations for the FeCoNiCuMo HEA and analyzed 1280 adsorption sites to develop ML models for predicting the adsorption energies of carboxyl (*COOH), *CO, and *CHO intermediates (Fig. 14(c)). Three optimized active sites (AS1–AS3) were selected for validation via DFT calculations (Figs. 14(d) and 14(e)). Full catalytic pathway analysis (Fig. 14(f)) demonstrated that AS1–AS3 exhibited limiting potentials of 0.37, 0.51, and 0.29 V, respectively, markedly superior to commercial catalysts (0.7 V). This breakthrough is attributed to the rotational freedom of *COOH and *CHO intermediates on HEA surfaces, which effectively bypasses traditional adsorption-energy scaling constraints.

Cavin et al. [115] reported a two-dimensional high-entropy transition metal dichalcogenide (TMDC) alloy, $(MoWVNbTa)S_2$ (Fig. 15(a)), which achieved over 90% CO selectivity at potentials of −0.16 to −0.31 V (vs. RHE) with a current density of 500 mA/cm^2. First-principles calculations revealed that its exceptional performance results from multi-site catalysis enabled by

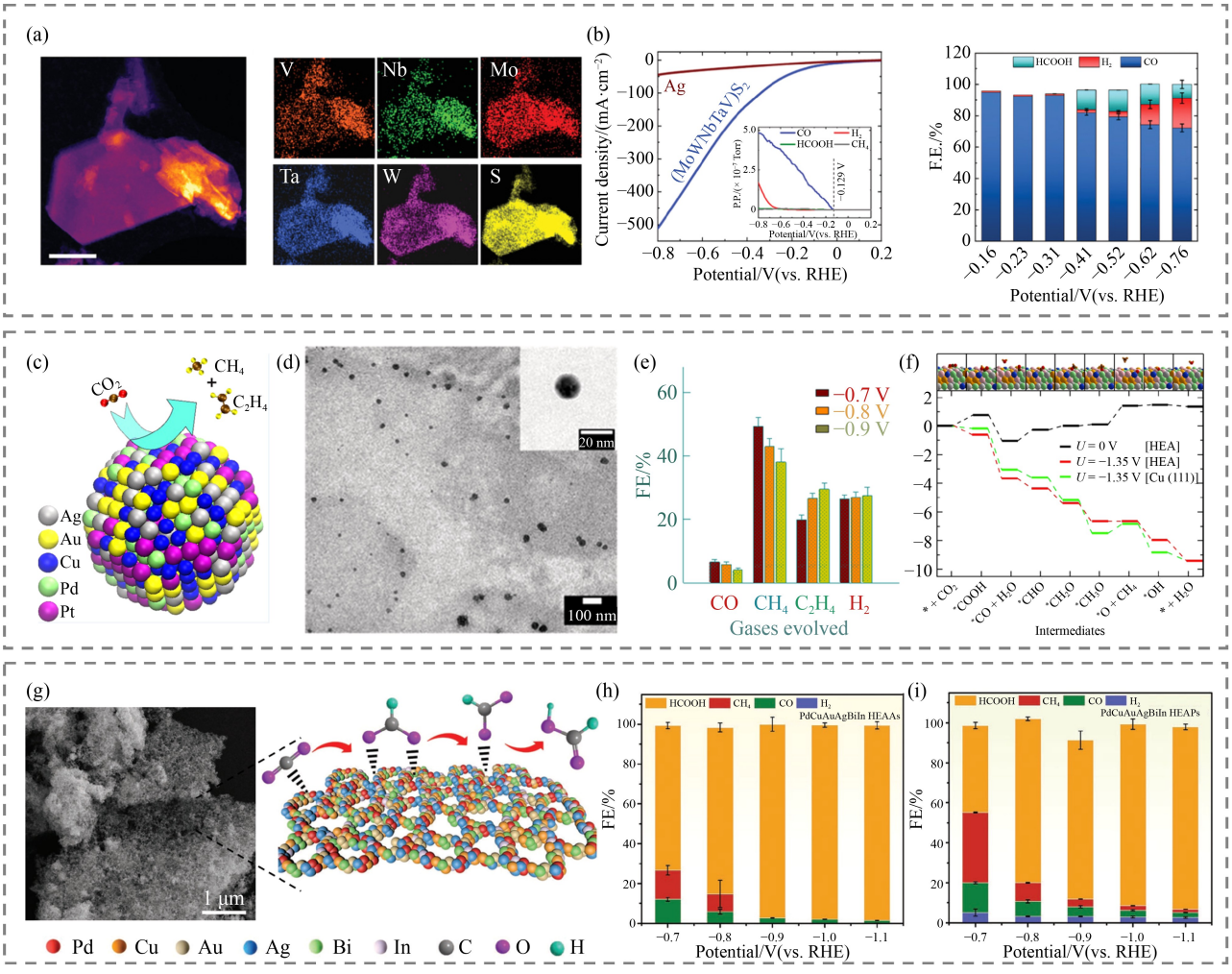

Fig. 15 Applications of HEAs in CO_2RR.

(a) HAADF-STEM and EDS images of high entropy nanosheet $(MoWVNbTa)S_2$, scale bar: 100 nm; (b) LSV and Faraday efficiency of high entropy nanosheet $(MoWVNbTa)S_2$ in CO_2RR (adapted with permission from Cavin et al. [115], copyright 2021, Wiley); (c) illustration of catalytic reactions on the AuAgPtPdCu HEA; (d) TEM bright-field image of HEA nanoparticles; (e) FE of various carbonaceous products and hydrogen produced during catalysis (adapted with permission from Nellaiappan et al. [125], copyright 2020, ACS Publications); (f) free energy diagram for CO_2RR on the surface of the AuAgPtPdCu HEA; (g) SEM image of PdCuAuAgBiIn HEAA and the reaction scheme; (h) performance plot of PdCuAuAgBiIn HEAs, showing the relationship between potential and FE for C_1 products; (i) performance comparison of PdCuAuAgBiIn HEA nanoparticles, indicating their efficiency and selectivity (adapted with permission from Li et al. [85], copyright 2023, Wiley).

atomic-scale disorder. The isolated transition metal edge sites weaken the CO binding strength (average desorption energy: 1.08 eV vs 1.55 eV for MoS_2), optimizing the rate-limiting CO desorption step (Fig. 15(b)). In contrast, Ag and VS_2 face a COOH* adsorption-dominated rate-limiting step, involving endothermic electron transfer. The negative free energy changes at the HEA sites favor reaction progression. This multi-metal synergy strikes a balance between moderate binding strength and reduced desorption energy, establishing a new paradigm for high-entropy material design.

Nellaiappan et al. [125] reported a nanocrystalline HEA catalyst, AuAgPtPdCu, averaging 16 nm in size (Figs. 15(c) and 15(d)), demonstrating great potential for the CO_2RR. At −0.3 V vs. RHE) the Faradaic efficiency for gaseous products, including CO, CH_4, C_2H_4, and H_2, approached nearly 100% (Fig. 15(e)). Notably, the formation of liquid-phase products was negligible, emphasizing the unique selectivity and efficiency of this HEA catalyst for CO_2RR. DFT calculations (Fig. 15(f)) demonstrated that the adsorption energies for the conversion of OCH_3 to an O intermediate on the HEA surface are markedly superior to those on pure copper surfaces. This finding indicates that the synergistic interactions among the various elements in the HEA are crucial for improving CO_2RR selectivity and efficiency.

HEA aerogels (HEAAs), which integrate the unique properties of HEAs and aerogels, represent a promising platform for advanced catalytic applications. Li et al. [85] developed a straightforward freeze-thaw synthesis method to produce HEAAs and prepared a series of HEAAs for CO_2RR. Among these, PdCuAuAgBiIn HEAAs exhibit a highly porous structure (Fig. 15(g)), as demonstrated by specific surface analysis. Owing to the synergistic interactions between the different metals and the high active surface area, PdCuAuAgBiIn HEAAs demonstrate outstanding CO_2RR performance. Notably, the Faradaic efficiency for formate (FE_{HCOOH}) of PdCuAuAgBiIn HEAAs reaches up to 98.1%, surpassing that of PdCuAuAgBiIn HEA particles (Figs. 15(h) and 15(i)). Furthermore, in a flow cell, the catalyst achieves a current density of approximately 200 mA/cm^2 and an FE_{HCOOH} of 87%, indicating exceptional formate selectivity. These remarkable properties are attributed to strong intermetallic interactions and surface unsaturated sites, which facilitate the adsorption and desorption of HCOO* intermediates. By altering the electronic configuration of different elements, these interactions significantly enhance formate selectivity and overall CO_2RR efficiency.

6 Outlook and summary

HEAs, with their diverse chemical compositions, optimized surface structures, high chemical stability, and resistance to poisoning, exhibit outstanding catalytic performance. As a novel class of catalysts, HEAs hold significant promise in reducing reliance on precious metals, enhancing catalytic efficiency, and advancing green energy technologies. However, their inherent complexity presents challenges, including difficulties in synthesis, intricate composition-performance relationships, and insufficient stability and reproducibility. To address these challenges, we have provided a series of strategies (Fig.16), and the specific strategies are as follows:

(1) Optimizing the size and morphology of HEAs

Optimizing the size and morphology of HEAs nanoparticles is an effective strategy to boost catalytic performance. The limited number of surface atoms in bulk alloys restricts their application in electrocatalysis. Reducing HEA particles to the nanoscale—or even atomic scale—maximizes the utilization of surface-active atoms. However, excessively small nanoparticles are prone to aggregation due to high surface energy, which reduces active site availability and diminishes performance. Therefore, achieving an optimal particle size that balances activity and stability is essential.

Additionally, the morphology can be typically modulated by controlling the number of active sites exposed at the catalytic reaction interface, thereby promoting the electrocatalytic efficiency [126].

Therefore adjusting the morphology of HEAs also plays a key role, including: ① 1D nanostructures (e.g., nanowires and nanorods): These provide a large aspect ratio, exposing more active sites, and increasing the surface area for reactant contact. ② 2D nanosheets: With ultra-thin thickness and large lateral dimensions, they significantly expose a substantial number of active sites and improve electrolyte contact, boosting catalytic efficiency. ③ 3D porous and hollow structures: These offer increased specific surface areas, utilizing both internal and external surfaces for enhanced catalytic performance.

(2) High-throughput experiments for HEAs screening

The element diversity in HEAs, along with their complex and varied component combinations, makes it challenging to identify and select the most active element combinations. High-throughput screening addresses this by rapidly and concurrently testing and analyzing a large number of samples or variables simultaneously. High-throughput experimentation can rapidly screen and analyze numerous alloy combinations, accelerating the study of composition-performance relationships. This technique typically involves automation, highly standardized processes, and powerful data processing capabilities. For instance, Shan et al. [127] developed a high-throughput method to prepare HEAs and evaluate their ORR performance. They first used a combination of micron-scale precursor array printing technology and

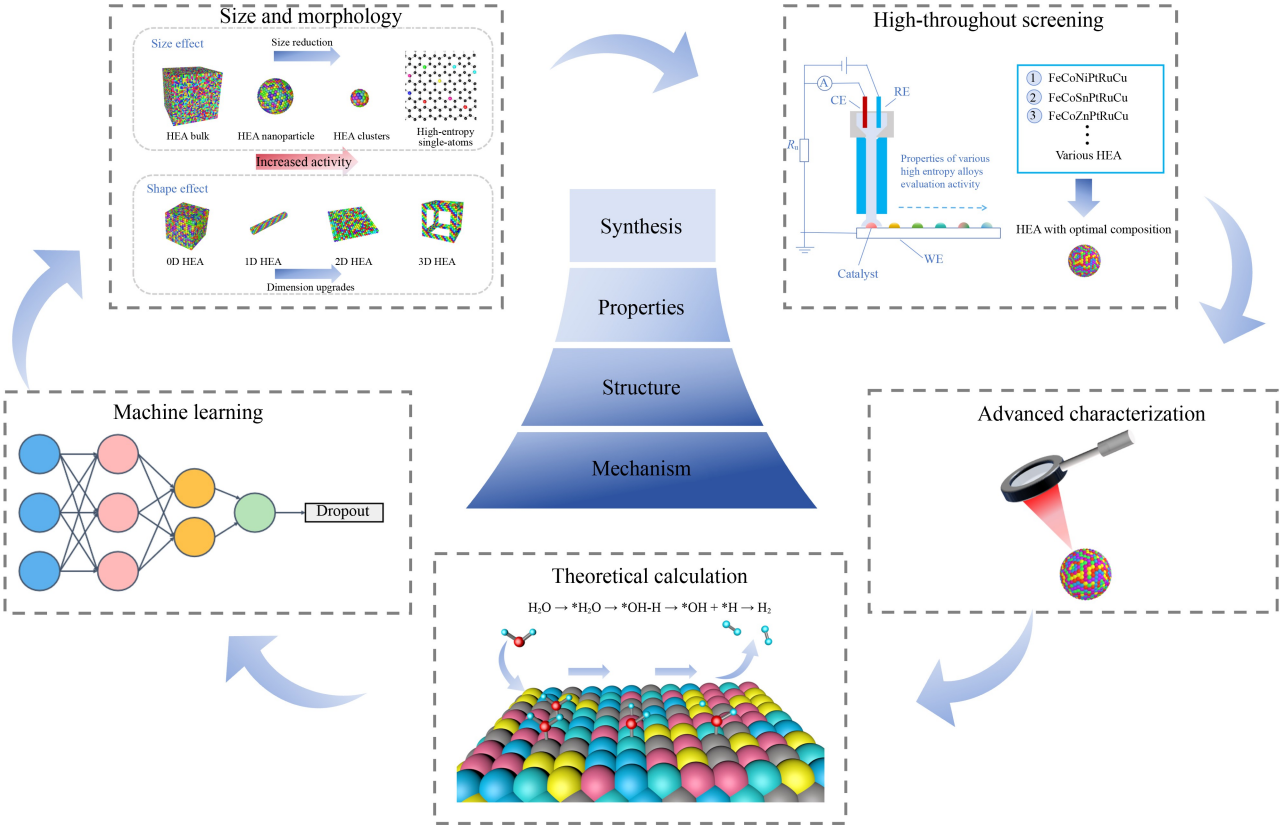

Fig. 16 Outlook of the development of HEAs.

pulsed high-temperature synthesis to rapidly generate HEA arrays with multiple element combinations. Programmatic high-throughput measurements enabled simultaneous analysis of 70 element combinations and 246 compositions in a single workday. This approach highlights the potential of high-throughput techniques to discover high-performing HEA catalysts efficiently.

(3) Advanced characterization techniques

Advanced characterization tools are essential for understanding the physical and chemical structures of HEAs. Key strategies include: ① **Atomic-resolution techniques**: Utilizing 4D STEM and synchrotron radiation for detailed structural and compositional analysis from nanoscale to atomic scale. ② **Multi-scale characterization**: Combining techniques such as APT and TEM to link microstructural features with macroscopic properties. ③ ***In situ* methods**: Employing *in situ* heating, stretching, and electrochemical characterization to study dynamic evolution under operational conditions.

(4) Improved theoretical calculation techniques

Developing efficient theoretical computational methods is crucial for exploring HEA mechanisms and structure-property relationships. Strategies include: ① **Novel hybrid models**: Combining first-principles calculations with statistical mechanics to better understand complex random solid solutions. ② **HEA databases**: Creating comprehensive databases for high-throughput screening to discover new alloys with targeted properties.

(5) ML predictions

Due to their complex multicomponent compositions and vast design space, HEAs are challenging to explore using traditional experimental and theoretical computational methods. ML, however, offers a powerful solution for navigating the vast compositional space of HEAs. HEAs can exhibit a variety of crystal structures (e.g., face-centered cubic, body-centered cubic, and amorphous phases) and surface defects. ML models, by extracting patterns from limited crystallographic data, can rapidly predict the stable structures of these complex systems. Furthermore, ML models are capable of fitting multidimensional data to effectively predict the catalytic activity of HEAs and uncover the associated correlations. For instance, Margraf et al. developed a multi-objective ML framework for HEAs, which optimizes activity, cost efficiency, and entropy stability simultaneously. Their ML model simulated the co-adsorption behavior of O and OH during ORR, enabling the identification of net adsorption enthalpy distributions and associated catalytic activities [128]. This method allows for the rapid identification of multiple promising ORR catalysts, achieving an optimized balance of objectives within an unexplored HEA design space containing up to 10 elements. Similarly, Chang et al. [129] simplified the

demand for DFT calculations utilizing ML, incorporating the similarity of adsorption sites into neural networks to reduce the number of data points required to achieve the desired accuracy. The results showed that the full DFT calculation workload was accelerated by a factor of 2, while maintaining the desired accuracy. Additionally, they experimentally validated the predicted $Fe_{0.125}Co_{0.125}Ni_{0.229}Ir_{0.229}Ru_{0.229}$ HEA electrocatalyst, which exhibited outstanding performance in ORR, outperforming traditional Pt/C catalysts.

In summary, as a novel material system, HEAs offer unique advantages and tremendous potential in electrocatalysis. Their diversified chemical compositions, complex crystal structures, and synergistic effects provide a broad design space for developing efficient electrocatalysts. While significant progress has been made, large-scale application of HEA electrocatalysts still faces numerous challenges, including optimizing preparation methods, gaining a deeper understanding of the structure-performance relationships, and ensuring long-term stability under practical application conditions. Future research should focus on low-cost, controllable synthesis techniques for HEAs, utilizing advanced characterization techniques, and improving theoretical calculations to reveal their catalytic mechanisms. Additionally, exploring the design principles of multifunctional HEA materials is essential to meet the demands of various electrocatalytic reactions. With continued multidisciplinary collaboration, HEAs are expected to play an increasingly important role in energy conversion and storage technologies, offering innovative solutions to global energy and environmental challenges.

Acknowledgements This work was supported by the National Natural Science Foundation of China (Grant No. 22302042), and the Pilot Group Program of the Research Fund for International Senior Scientists (Grant No. 22250710676).

Competing Interests Jiujun Zhang is the Deputy Editor-in-Chief of Frontiers in Energy, Wei Yan is a member of Editorial Board of Frontiers in Energy who were excluded from the peer-review process and all editorial decisions related to the acceptance and publication of this article. Peer-review was handled independently by the other editors to minimise bias.

References

1. Tang C, Zheng Y, Jaroniec M, et al. Electrocatalytic refinery for sustainable production of fuels and chemicals. Angewandte Chemie International Edition, 2021, 60(36): 19572–19590
2. He M, Sun Y, Han B. Green carbon science: Efficient carbon resource processing, utilization, and recycling towards carbon neutrality. Angewandte Chemie International Edition, 2022, 61(15): e202112835
3. Chu S, Majumdar A. Opportunities and challenges for a sustainable energy future. Nature, 2012, 488(7411): 294–303
4. Lewis N S, Nocera D G. Powering the planet: Chemical challenges in solar energy utilization. Proceedings of the National Academy of Sciences of the United States of America, 2006, 103(43): 15729–15735
5. Pashchenko D. Green hydrogen as a power plant fuel: What is energy efficiency from production to utilization? Renewable Energy, 2024, 223: 120033
6. Karayel G K, Dincer I. Green hydrogen production potential of Canada with solar energy. Renewable Energy, 2024, 221: 119766
7. Gasteiger H A, Kocha S S, Sompalli B, et al. Activity benchmarks and requirements for Pt, Pt-alloy, and non-Pt oxygen reduction catalysts for PEMFCs. Applied Catalysis B: Environmental, 2005, 56(1−2): 9–35
8. Jiao Y, Zheng Y, Jaroniec M, et al. Design of electrocatalysts for oxygen- and hydrogen-involving energy conversion reactions. Chemical Society Reviews, 2015, 44(8): 2060–2086
9. Turner J A. Sustainable hydrogen production. Science, 2004, 305: 972–974
10. Kim S, Shin S J, Kim H, et al. Self-assembly-assisted dynamic placement of noble metals selectively on multifunctional carbide supports for alkaline hydrogen electrocatalysis. Energy & Environmental Science, 2025, 18(2): 659–673
11. Tian L, Li Z, Xu X, et al. Advances in noble metal (Ru, Rh, and Ir) doping for boosting water splitting electrocatalysis. Journal of Materials Chemistry. A, Materials for Energy and Sustainability, 2021, 9(23): 13459–13470
12. Kong W, Deng J, Li L. Recent advances in noble metal MXene-based catalysts for electrocatalysis. Journal of Materials Chemistry. A, Materials for Energy and Sustainability, 2022, 10(28): 14674–14691
13. Chang H, Shi L N, Chen Y H, et al. Advanced MOF-derived carbon-based non-noble metal oxygen electrocatalyst for next-generation rechargeable Zn-air batteries. Coordination Chemistry Reviews, 2022, 473: 214839
14. Wang T, Xie H, Chen M, et al. Precious metal-free approach to hydrogen electrocatalysis for energy conversion: From mechanism understanding to catalyst design. Nano Energy, 2017, 42: 69–89
15. Narendra Kumar A V, Muthu Prabhu S, Shin W S, et al. Prospects of non-noble metal single atoms embedded in two-dimensional (2D) carbon and non-carbon-based structures in electrocatalytic applications. Coordination Chemistry Reviews, 2022, 467: 214613
16. Xin Y, Li S, Qian Y, et al. High-entropy alloys as a platform for catalysis: Progress, challenges, and opportunities. ACS Catalysis, 2020, 10(19): 11280–11306
17. Ma Y, Ma Y, Wang Q, et al. High-entropy energy materials: Challenges and new opportunities. Energy & Environmental Science, 2021, 14(5): 2883–2905
18. Sun Y, Dai S. High-entropy materials for catalysis: A new frontier. Science Advances, 2021, 7(20): eabg1600
19. George E P, Raabe D, Ritchie R O. High-entropy alloys. Nature Reviews. Materials, 2019, 4(8): 515–534
20. Yeh J W, Chen S K, Lin S J, et al. Nanostructured high-entropy alloys with multiple principal elements: Novel alloy design concepts and outcomes. Advanced Engineering Materials, 2004, 6(5): 299–303

21. Niu B, Zhang F, Ping H, et al. Sol-gel autocombustion synthesis of nanocrystalline high-entropy alloys. Scientific Reports, 2017, 7(1): 3421
22. Li H, Lai J, Li Z, et al. Multi-sites electrocatalysis in high-entropy alloys. Advanced Functional Materials, 2021, 31(47): 2106715
23. Yu L, Zeng K, Li C, et al. High-entropy alloy catalysts: From bulk to nano toward highly efficient carbon and nitrogen catalysis. Carbon Energy, 2022, 4(5): 731–761
24. Li K, Chen W. Recent progress in high-entropy alloys for catalysts: Synthesis, applications, and prospects. Materials Today. Energy, 2021, 20: 100638
25. Huo X, Yu H, Xing B, et al. Review of high entropy alloys electrocatalysts for hydrogen evolution, oxygen evolution, and oxygen reduction reaction. Chemical Record, 2022, 22(12): e202200175
26. Yao Y, Dong Q, Brozena A, et al. High-entropy nanoparticles: Synthesis-structure-property relationships and data-driven discovery. Science, 2022, 376(6589): eabn3103
27. Zhang Y, Wang D, Wang S. High-entropy alloys for electrocatalysis: Design, characterization, and applications. Small, 2022, 18(7): 2104339
28. Ren J T, Chen L, Wang H Y, et al. High-entropy alloys in electrocatalysis: From fundamentals to applications. Chemical Society Reviews, 2023, 52(23): 8319–8373
29. Ma Y, Ma Y, Wang Q, et al. High-entropy energy materials: Challenges and new opportunities. Energy & Environmental Science, 2021, 14(5): 2883–2905
30. Al Zoubi W, Putri R A K, Abukhadra M R, et al. Recent experimental and theoretical advances in the design and science of high-entropy alloy nanoparticles. Nano Energy, 2023, 110: 108362
31. Yao Y, Dong Q, Brozena A, et al. High-entropy nanoparticles: Synthesis-structure-property relationships and data-driven discovery. Science, 2022, 376(6589): eabn3103
32. Zhai Y, Ren X, Wang B, et al. High-entropy catalyst—A novel platform for electrochemical water splitting. Advanced Functional Materials, 2022, 32(47): 2207536
33. Sun Y, Dai S. High-entropy materials for catalysis: A new frontier. Science Advances, 2021, 7: eabg1600
34. Seh Z W, Kibsgaard J, Dickens C F, et al. Combining theory and experiment in electrocatalysis: Insights into materials design. Science, 2017, 355(6321): eaad4998
35. Wang B, Yao Y, Yu X, et al. Understanding the enhanced catalytic activity of high entropy alloys: From theory to experiment. Journal of Materials Chemistry. A, Materials for Energy and Sustainability, 2021, 9(35): 19410–19438
36. Ma Y, Kou Z, Yang W, et al. A one-step fabrication of soft-magnetic high entropy alloy fiber with excellent strength and flexibility. Nature Communications, 2024, 15(1): 10549
37. Mori K, Hashimoto N, Kamiuchi N, et al. Hydrogen spillover-driven synthesis of high-entropy alloy nanoparticles as a robust catalyst for CO_2 hydrogenation. Nature Communications, 2021, 12(1): 3884
38. Liu H, Zhang Y, Zhang L, et al. Unveiling atomic-scaled local chemical order of high-entropy intermetallic catalyst for alkyl-substitution-dependent alkyne semihydrogenation. Journal of the American Chemical Society, 2024, 146(29): 20193–20204
39. Nakaya Y, Hayashida E, Asakura H, et al. High-entropy intermetallics serve ultrastable single-atom Pt for propane dehydrogenation. Journal of the American Chemical Society, 2022, 144(35): 15944–15953
40. Löffler T, Ludwig A, Rossmeisl J, et al. What makes high-entropy alloys exceptional electrocatalysts? Angewandte Chemie International Edition, 2021, 60(52): 26894–26903
41. Chen T, Qiu C, Zhang X, et al. An ultrasmall ordered high-entropy intermetallic with multiple active sites for the oxygen reduction reaction. Journal of the American Chemical Society, 2024, 146(1): 1174–1184
42. Feng G, Pan Y, Su D, et al. Constructing fully-active and ultra-active sites in high-entropy alloy nanoclusters for hydrazine oxidation-assisted electrolytic hydrogen production. Advanced Materials, 2024, 36(13): 2309715
43. Broge N L N, Bertelsen A D, Søndergaard-Pedersen F, et al. Facile solvothermal synthesis of Pt–Ir–Pd–Rh–Ru–Cu–Ni–Co high-entropy alloy nanoparticles. Chemistry of Materials, 2023, 35(1): 144–153
44. Chen H, Guan C, Feng H. Pt-based high-entropy alloy nanoparticles as bifunctional electrocatalysts for hydrogen and oxygen evolution. ACS Applied Nano Materials, 2022, 5(7): 9810–9817
45. Wang Y, Luo W, Gong S, et al. Synthesis of high-entropy-alloy nanoparticles by a step-alloying strategy as a superior multifunctional electrocatalyst. Advanced Materials, 2023, 35(36): 2302499
46. Sun X, Sun Y. Synthesis of metallic high-entropy alloy nanoparticles. Chemical Society Reviews, 2024, 53(9): 4400–4433
47. Wang Z L, Huang G Y, Zhu G R, et al. La-exacerbated lattice distortion of high entropy alloys for enhanced electrocatalytic water splitting. Applied Catalysis B: Environment and Energy, 2025, 361: 124585
48. Li Z, Wu R, Duan D, et al. Empowering multicomponent alloys with unique nanostructure for exceptional oxygen evolution performance through self-replenishment. Joule, 2024, 8(10): 2920–2937
49. Wang H, He Q, Gao X, et al. Multifunctional high entropy alloys enabled by severe lattice distortion. Advanced Materials, 2024, 36(17): 2305453
50. Wang Y, Meng H, Yu R, et al. Unconventional interconnected high-entropy alloy nanodendrites for remarkably efficient C–C bond cleavage toward complete ethanol oxidation. Angewandte Chemie International Edition, 2024, 137(10): e202420752
51. Zhu H, Sun S, Hao J, et al. A high-entropy atomic environment converts inactive to active sites for electrocatalysis. Energy & Environmental Science, 2023, 16(2): 619–628
52. Zhang Z J, Guo J P, Sun S H, et al. Optimized valence state of Co and Ni in high-entropy alloy for high active-stable OER. Rare Metals, 2023, 42(11): 3607–3613
53. Zou X, Zhao X, Pang B, et al. Interstitial oxygen acts as electronic buffer stabilizing high-entropy alloys for trifunctional electrocatalysis. Advanced Materials, 2024, 36(50): 2412954

54. Huang K, Xia J, Lu Y, et al. Self-reconstructed spinel surface structure enabling the long-term stable hydrogen evolution reaction/oxygen evolution reaction efficiency of FeCoNiRu high-entropy alloyed electrocatalyst. Advanced Science, 2023, 10(14): 2300094
55. Yao Y, Huang Z, Xie P, et al. Carbothermal shock synthesis of high-entropy-alloy nanoparticles. Science, 2018, 359(6383): 1489–1494
56. Zeng K, Zhang J, Gao W, et al. Surface-decorated high-entropy alloy catalysts with significantly boosted activity and stability. Advanced Functional Materials, 2022, 32(33): 2204643
57. Yao Y, Huang Z, Li T, et al. High-throughput, combinatorial synthesis of multimetallic nanoclusters. Proceedings of the National Academy of Sciences of the United States of America, 2020, 117(12): 6316–6322
58. Xie P, Yao Y, Huang Z, et al. Highly efficient decomposition of ammonia using high-entropy alloy catalysts. Nature Communications, 2019, 10(1): 4011
59. Wang G, Li L, Zhang S, et al. Preparation of graphene-coated high entropy alloy nanoparticles by double pulse carbothermal shock. Scripta Materialia, 2023, 236: 115668
60. Hu C, Zhang Y, Ren R, et al. A selenium-mediated layer-by-layer synthetic strategy for multilayered multicomponent nanocrystals. Nature Synthesis, 2024, 3(10): 1299–1309
61. Vinnacombe-Willson G A, Conti Y, Stefancu A, et al. Direct bottom-up *in situ* growth: A paradigm shift for studies in wet-chemical synthesis of gold nanoparticles. Chemical Reviews, 2023, 123(13): 8488–8529
62. Luo H, Li L, Lin F, et al. Sub-2 nm microstrained high-entropy-alloy nanoparticles boost hydrogen electrocatalysis. Advanced Materials, 2024, 36(32): 2403674
63. He R, Wang S, Yang L, et al. Active site switching on high entropy phosphides as bifunctional oxygen electrocatalysts for rechargeable/robust Zn–air battery. Energy & Environmental Science, 2024, 17(19): 7193–7208
64. Liu M, Zhang Z, Okejiri F, et al. Entropy-maximized synthesis of multimetallic nanoparticle catalysts via a ultrasonication-assisted wet chemistry method under ambient conditions. Advanced Materials Interfaces, 2019, 6(7): 1900015
65. Nandan R, Nara H, Nam H N, et al. Tailored design of mesoporous nanospheres with high entropic alloy sites for efficient redox electrocatalysis. Advanced Science, 2024, 11(35): 2402518
66. Huang K, Zhang B, Wu J, et al. Exploring the impact of atomic lattice deformation on oxygen evolution reactions based on a sub-5 nm pure face-centred cubic high-entropy alloy electrocatalyst. Journal of Materials Chemistry. A, Materials for Energy and Sustainability, 2020, 8(24): 11938–11947
67. Minamihara H, Kusada K, Wu D, et al. Continuous-flow reactor synthesis for homogeneous 1 nm-sized extremely small high-entropy alloy nanoparticles. Journal of the American Chemical Society, 2022, 144(26): 11525–11529
68. Huang Y, Chen Y, Xu M, et al. Catalysts by pyrolysis: Transforming metal-organic frameworks (MOFs) precursors into metal-nitrogen-carbon (M-N-C) materials. Materials Today, 2023, 69: 66–78
69. Cai Z, Wang Z, Kim J, et al. Hollow functional materials derived from metal–organic frameworks: Synthetic strategies, conversion mechanisms, and electrochemical applications. Advanced Materials, 2019, 31(11): 1804903
70. Watt W. Pyrolysis of polyacrylonitrile. Nature, 1969, 222(5190): 265–266
71. Chen Y, Wang C, Wu Z, et al. Metal-organic frameworks: From bimetallic metal-organic framework to porous carbon: high surface area and multicomponent active dopants for excellent electrocatalysis. Advanced Materials, 2015, 27(34): 5010–5016
72. Kar N, McCoy M, Wolfe J, et al. Retrosynthetic design of core-shell nanoparticles for thermal conversion to monodisperse high-entropy alloy nanoparticles. Nature Synthesis, 2023, 3(2): 175–184
73. Qiu Z, Li Y, Gao Y, et al. 2D MOF-assisted pyrolysis-displacement-alloying synthesis of high-entropy alloy nanoparticles library for efficient electrocatalytic hydrogen oxidation. Angewandte Chemie International Edition, 2023, 62(33): e202306881
74. Zhang W, Feng X, Mao Z X, et al. Stably immobilizing sub-3 nm high-entropy Pt alloy nanocrystals in porous carbon as durable oxygen reduction electrocatalyst. Advanced Functional Materials, 2022, 32(44): 2204110
75. Rao P, Deng Y, Fan W, et al. Movable type printing method to synthesize high-entropy single-atom catalysts. Nature Communications, 2022, 13(1): 5071
76. Mori K, Hashimoto N, Kamiuchi N, et al. Hydrogen spillover-driven synthesis of high-entropy alloy nanoparticles as a robust catalyst for CO_2 hydrogenation. Nature Communications, 2021, 12(1): 3884
77. Gao S, Hao S, Huang Z, et al. Synthesis of high-entropy alloy nanoparticles on supports by the fast moving bed pyrolysis. Nature Communications, 2020, 11(1): 2016
78. Wang X, Dong Q, Qiao H, et al. Continuous synthesis of hollow high-entropy nanoparticles for energy and catalysis applications. Advanced Materials, 2020, 32(46): 2002853
79. Wang B, Wang C, Yu X, et al. General synthesis of high-entropy alloy and ceramic nanoparticles in nanoseconds. Nature Synthesis, 2022, 1(2): 138–146
80. Zhong G, Xu S, Chen C, et al. Synthesis of metal oxide nanoparticles by rapid, high-temperature 3D microwave heating. Advanced Functional Materials, 2019, 29(48): 1904282
81. Zhao H, Yuan Y, Zhang D, et al. Ultrafast generation of nanostructured noble metal aerogels by a microwave method for electrocatalytic hydrogen evolution and ethanol oxidation. ACS Applied Nano Materials, 2021, 4(10): 11221–11230
82. Qiao H, Saray M T, Wang X, et al. Scalable synthesis of high entropy alloy nanoparticles by microwave heating. ACS Nano, 2021, 15(9): 14928–14937
83. Löffler T, Meyer H, Savan A, et al. Discovery of a multinary noble metal-free oxygen reduction catalyst. Advanced Energy Materials, 2018, 8(34): 1802269
84. Manjón A G, Löffler T, Meischein M, et al. Sputter deposition of highly active complex solid solution electrocatalysts into an ionic liquid library: Effect of structure and composition on oxygen reduction activity. Nanoscale, 2020, 12(46):

23570–23577
85. Li H, Huang H, Chen Y, et al. High-entropy alloy aerogels: A new platform for carbon dioxide reduction. Advanced Materials, 2023, 35(2): 2209242
86. Yang Y, Zhou J, Zhu F, et al. Determining the three-dimensional atomic structure of an amorphous solid. Nature, 2021, 592(7852): 60–64
87. Cao G, Liang J, Guo Z, et al. Liquid metal for high-entropy alloy nanoparticles synthesis. Nature, 2023, 619(7968): 73–77
88. Hao J, Zhuang Z, Cao K, et al. Unraveling the electronegativity-dominated intermediate adsorption on high-entropy alloy electrocatalysts. Nature Communications, 2022, 13(1): 2662
89. Lu Y, Zhu M, Chen S, et al. Single-atom Fe-catalyzed acceptorless dehydrogenative coupling to quinolines. Journal of the American Chemical Society, 2024, 146(33): 23338–23347
90. Wu D, Kusada K, Nanba Y, et al. Noble-metal high-entropy-alloy nanoparticles: Atomic-level insight into the electronic structure. Journal of the American Chemical Society, 2022, 144(8): 3365–3369
91. Song B, Yang Y, Rabbani M, et al. *In situ* oxidation studies of high-entropy alloy nanoparticles. ACS Nano, 2020, 14(11): 15131–15143
92. He Y, Liu S, Wang M, et al. Advanced *In situ* characterization techniques for direct observation of gas-involved electrochemical reactions. Energy & Environmental Materials, 2023, 6(6): e12552
93. Cheng W, Zhao X, Su H, et al. Lattice-strained metal–organic-framework arrays for bifunctional oxygen electrocatalysis. Nature Energy, 2019, 4(2): 115–122
94. Zhao Y, Adiyeri Saseendran D P, Huang C, et al. Oxygen evolution/reduction reaction catalysts: From *in situ* monitoring and reaction mechanisms to rational design. Chemical Reviews, 2023, 123(9): 6257–6358
95. Ge X, Sumboja A, Wuu D, et al. Oxygen reduction in alkaline media: from mechanisms to recent advances of catalysts. ACS Catalysis, 2015, 5(8): 4643–4667
96. Sun Y, Sun S, Yang H, et al. Spin-related electron transfer and orbital interactions in oxygen electrocatalysis. Advanced Materials, 2020, 32(39): 2003297
97. Guo Y, Shang C, Li J, et al. Recent development of hydrogen evolution, oxygen evolution and oxygen reduction reaction. Scientia Sinica Chimica, 2018, 48(8): 926–940 (in Chinese)
98. Wang K, Chen R, Yang H, et al. The elements selection of high entropy alloy guided by thermodynamics and the enhanced electrocatalytic mechanism for oxygen reduction reaction. Advanced Functional Materials, 2024, 34(7): 2310683
99. Zuo X, Yan R, Zhao L, et al. A hollow PdCuMoNiCo high-entropy alloy as an efficient bi-functional electrocatalyst for oxygen reduction and formic acid oxidation. Journal of Materials Chemistry. A, Materials for Energy and Sustainability, 2022, 10(28): 14857–14865
100. Zhao X, Cheng H, Chen X, et al. Multiple metal-nitrogen bonds synergistically boosting the activity and durability of high-entropy alloy electrocatalysts. Journal of the American Chemical Society, 2024, 146(5): 3010–3022
101. Xie M, Lu Y, Xiao X, et al. Spatially immobilized PtPdFeCoNi as an excellent bifunctional oxygen electrocatalyst for zinc-air battery. Advanced Functional Materials, 2024, 35(5): 2414537
102. Zhu J, Hu L, Zhao P, et al. Recent advances in electrocatalytic hydrogen evolution using nanoparticles. Chemical Reviews, 2020, 120(2): 851–918
103. Sun F, Tang Q, Jiang D. Theoretical advances in understanding and designing the active sites for hydrogen evolution reaction. ACS Catalysis, 2022, 12(14): 8404–8433
104. Cheng W, Zhao X, Su H, et al. Lattice-strained metal-organic-framework arrays for bifunctional oxygen electrocatalysis. Nature Energy, 2019, 4(2): 115–122
105. Zhou L, Lu S, Guo S. Recent progress on precious metal single atom materials for water splitting catalysis. SusMat, 2021, 1(2): 194–210
106. Cheng Q Y, Wang M F, Ni J J, et al. High-entropy alloys for accessing hydrogen economy via sustainable production of fuels and direct application in fuel cells. Rare Metals, 2023, 42(11): 3553–3569
107. Zhou M, Li C, Fang J. Noble-metal based random alloy and intermetallic nanocrystals: Syntheses and applications. Chemical Reviews, 2021, 121(2): 736–795
108. Li Y, Peng C K, Sun Y, et al. Operando elucidation of hydrogen production mechanisms on sub-nanometric high-entropy metallenes. Nature Communications, 2024, 15(1): 10222
109. Wang S, Xu B, Huo W, et al. Efficient FeCoNiCuPd thin-film electrocatalyst for alkaline oxygen and hydrogen evolution reactions. Applied Catalysis B: Environmental, 2022, 313: 121472
110. Zhao H, Liu M, Wang Q, et al. Strong transboundary electron transfer of high-entropy quantum-dots driving rapid hydrogen evolution kinetics. Energy & Environmental Science, 2024, 17(18): 6594–6605
111. Kang Y, Cretu O, Kikkawa J, et al. Mesoporous multimetallic nanospheres with exposed highly entropic alloy sites. Nature Communications, 2023, 14(1): 4182
112. Chen Z W, Li J, Ou P, et al. Unusual Sabatier principle on high entropy alloy catalysts for hydrogen evolution reactions. Nature Communications, 2024, 15(1): 359
113. Nellaiappan S, Katiyar N K, Kumar R, et al. High-entropy alloys as catalysts for the CO_2 and CO reduction reactions: Experimental realization. ACS Catalysis, 2020, 10(6): 3658–3663
114. Cai W, Cao X, Wang Y, et al. Spatial structure of electron interactions in high-entropy oxide nanoparticles for active electrocatalysis of carbon dioxide reduction. Advanced Materials, 2024, 36(45): 2409949
115. Cavin J, Ahmadiparidari A, Majidi L, et al. 2D high-entropy transition metal dichalcogenides for carbon dioxide electrocatalysis. Advanced Materials, 2021, 33(31): 2100347
116. Ostovari Moghaddam A, Mehrabi-Kalajahi S, Abdollahzadeh A, et al. High-entropy $La(FeCuMnMgTi)O_3$ nanoparticles as heterogeneous catalyst for CO_2 electroreduction reaction. Journal of Physical Chemistry Letters, 2024, 15(20): 5535–5542
117. Chang B, Pang H, Raziq F, et al. Electrochemical reduction of carbon dioxide to multicarbon (C_{2+}) products: Challenges and perspectives. Energy & Environmental Science, 2023, 16(11):

4714–4758

118. Wang G, Chen J, Ding Y, et al. Electrocatalysis for CO_2 conversion: From fundamentals to value-added products. Chemical Society Reviews, 2021, 50(8): 4993–5061
119. Nam D H, De Luna P, Rosas-Hernández A, et al. Molecular enhancement of heterogeneous CO_2 reduction. Nature Materials, 2020, 19(3): 266–276
120. Du Y, Meng X, Ma Y, et al. Dimensionality engineering toward carbon materials for electrochemical CO_2 reduction: Progress and prospect. Advanced Functional Materials, 2024, 34(46): 2408013
121. Liu L, Akhoundzadeh H, Li M, et al. Alloy catalysts for electrocatalytic CO_2 reduction. Small Methods, 2023, 7(9): 2300482
122. Roy D, Mandal S C, Pathak B. Machine learning assisted exploration of high entropy alloy-based catalysts for selective CO_2 reduction to methanol. Journal of Physical Chemistry Letters, 2022, 13(25): 5991–6002
123. Pedersen J K, Batchelor T A A, Bagger A, et al. High-entropy alloys as catalysts for the CO_2 and CO reduction reactions. ACS Catalysis, 2020, 10(3): 2169–2176
124. Chen Z W, Gariepy Z, Chen L, et al. Machine-learning-driven high-entropy alloy catalyst discovery to circumvent the scaling relation for CO_2 reduction reaction. ACS Catalysis, 2022, 12(24): 14864–14871
125. Nellaiappan S, Katiyar N K, Kumar R, et al. High-entropy alloys as catalysts for the CO_2 and CO reduction reactions: Experimental realization. ACS Catalysis, 2020, 10(6): 3658–3663
126. He Y, Liu S, Wang M, et al. Deciphering engineering principle of three-phase interface for advanced gas-involved electrochemical reactions. Journal of Energy Chemistry, 2023, 80: 302–323
127. Shan X, Pan Y, Cai F, et al. Accelerating the discovery of efficient high-entropy alloy electrocatalysts: High-throughput experimentation and data-driven strategies. Nano Letters, 2024, 24(37): 11632–11640
128. Xu W, Diesen E, He T, et al. Discovering high entropy alloy electrocatalysts in vast composition spaces with multiobjective optimization. Journal of the American Chemical Society, 2024, 146(11): 7698–7707
129. Chang Y, Benlolo I, Bai Y, et al. High-entropy alloy electrocatalysts screened using machine learning informed by quantum-inspired similarity analysis. Matter, 2024, 7(11): 4099–4113